cxcl18b-defined transitional state-specific nitric oxide drives injury-induced Müller glia cell-cycle re-entry in the zebrafish retina

Aojun Ye[1,3], Shuguang Yu[2], Meng Du[4], Dongming Zhou[4], Jie He[2,*] and Chang Chen[1,3,5,*]

[1]National Laboratory of Biomacromolecules, CAS Center for Excellence in Biomacromolecules, Institute of Biophysics, Chinese Academy of Sciences, Beijing 100101, China

[2]Institute of Neuroscience, State Key Laboratory of Neuroscience, CAS Center for Excellence in Brain Science and Intelligence Technology, Chinese Academy of Sciences, Shanghai 200031, China

[3]University of Chinese Academy of Sciences, Beijing 100049, China

[4]Tianjin Medical University, Tianjin 300070, China

[5]Lead contact

*Correspondence: jiehe@ion.ac.cn, changchen@moon.ibp.ac.cn

Abstract:

In lower vertebrates, retinal Müller glia (MG) exhibit a life-long capacity of cell-cycle re-entry to regenerate neurons following the retinal injury. However, the mechanism driving such injury-induced MG cell-cycle re-entry remains incompletely understood. Combining single-cell transcriptomic analysis and *in-vivo* clonal analysis, we identified previously undescribed *cxcl18b*-defined MG transitional states as essential routes towards MG proliferation following green/red cone (G/R cone) ablation. Microglial inflammation was necessary for triggering these transitional states, which expressed the gene modules shared by cells of the ciliary marginal zone (CMZ) where life-long adult neurogenesis takes place. Functional studies of the redox

properties of these transitional states further demonstrated the regulatory role of nitric oxide (NO) produced by *Nos2b* in injury-induced MG proliferation. Finally, we developed a viral-based strategy to specifically disrupt *nos2b* in *cxcl18b*-defined MG transitional states and revealed the effect of transitional state-specific NO signaling. Our findings elucidate the redox-related mechanism underlying injury-induced MG cell-cycle re-entry, providing insights into species-specific mechanisms for vertebrate retina regeneration.

Key Words: Müller glia, zebrafish retina, cell cycle re-entry, nitric oxide, *cxcl18b*.

Introduction:

Unlike mammalian counterparts, retinal Müller glia (MG) of aquatic and amphibian species can enter injury-induced regeneration program**(Goldman, 2014; Lahne et al., 2020b; Wan and Goldman, 2016)**, which unfolds a set of temporal events from glial reactivation, glial proliferation, new neuron generation, and circuit integration**(Abraham et al., 2024; Powell et al., 2016)**. The initial glial reactivation is highly conversed across species, from lower vertebrates to mammals, with the characteristic glial expression of *ascl1α, lin28a, sox2*, and *mycb/h* and increased morphological complexity**(Gorsuch et al., 2017; Jorstad et al., 2017; Lee et al., 2024; Ramachandran et al., 2010).** Diverse signaling pathways have been identified to participate in this initial glial reactivation**(Campbell et al., 2021; Wan and Goldman, 2017).**

In contrast, our knowledge of the mechanism underlying injury-induced glial cell-cycle re-entry, a critical step for neuron regeneration specific to aquatic and

amphibian species but not mammals**(Lenkowski and Raymond, 2014; Vihtelic and Hyde, 2000; Wu et al., 2001)**, remains limited. Even in the case of an enforced proliferation by over-expressing cell-cycle regulators, MG can undergo gliogenesis rather than neurogenesis in the rat retina**(Close et al., 2005; Close et al., 2006; Nishino et al., 2023)**. The mechanistic understanding of MG cell-cycle re-entry in the injured zebrafish retina will provide critical knowledge for inspiring new strategies for *in-vivo* re-programming MG to repair the human retina.

The intrinsic and environmental factors contribute to injury-induced MG proliferation**(Gao et al., 2021; Lahne et al., 2020b; Xiao et al., 2023)**. Recent efforts in single-cell RNA-sequencing (scRNA-Seq) have identified *ascl1α*, *clcf1*/*crlf1a***(Boyd et al., 2023)**, and *mycb*/*mych***(Lee et al., 2024)** as key intrinsic drivers of injury-induced MG proliferation in the zebrafish retina. Also, the elegant study of MG injury responses across multiple species, including zebrafish, chicken, and mice, revealed the *hmga1/yap1* signaling network as a key regulator of MG reprogramming and neurogenesis in the regenerating retina**(Hoang et al., 2020).** Interestingly, previous studies further reported that post-injury MG in the zebrafish are capable of re-acquiring the regeneration program that largely recapitulates the embryonic retinal developmental program**(Celotto et al., 2023; Hoang et al., 2020; Lahne et al., 2020a; Lyu et al., 2023)**.

In terms of extrinsic cues, two sources, those from damaged neurons and injury-recruited microglia, are considered indispensable for injury-induced MG proliferation**(Leach et al., 2021; White et al., 2017)**. Previous studies have shown

that signals derived from various retinal neuron injury models trigger MG regeneration, each exerting distinct effects on MG reprogramming**(Lyu et al., 2023)**. Meanwhile, accumulative evidence increasingly appreciates the role of inflammatory signals derived from injury-recruited microglia, such as *TNFα***(Conner et al., 2014; Nelson et al., 2013)**, cytokines IL-1β, and IL-10**(Lu and Hyde, 2024)**. Notably, inflammatory responses are intrinsically associated with redox signaling, which is involved in the regeneration processes in various non-neuronal tissues**(Breus and Dickmeis, 2021; Jaeschke, 2000; Zhang et al., 2024)**. However, the involvement of the redox signaling resulted from microglia-derived inflammatory signals in MG cell-cycle re-entry following retina damage remains to be clarified. Nitric oxide (NO), a redox signal, has participated in regenerating various tissues in zebrafish, including the heart**(Rochon et al., 2020; Yu et al., 2024)**, spinal cord**(Bradley et al., 2010)**, and fin**(Matrone et al., 2021)**. Endogenous NO is derived from three forms of NO synthase (NOS) in mammalians: neuronal NOS (nNOS), endothelial NOS (eNOS), and inducible NOS (iNOS). The zebrafish comprises *Nos1*, a form of neuronal *Nos*, and *Nos2a*/*2b*, two inducible *Nos*.

In this study, we performed single-cell RNA sequencing to characterize the post-injury MG states in the zebrafish retina following the specific ablation of green/red cone. This comprehensive analysis led us to define a set of previously unknown *cxcl18b* positive transitional states as an essential route of MG cell-cycle re-entry in response to the injury, and the inflammatory reactions of recruited microglia were indispensable for the induction of these transitional states. Intriguingly, we found

these *cxcl18b*-defined transitional states exhibited gene patterns shared by cell states in the CMZ, favoring the idea that *cxcl18b*-defined MG transitional states might represent the developmental program conserved by neuronal regeneration beyond the embryonic development. A remarkable phenotype of enriched redox features in these gene patterns suggested the importance of redox signaling. The subsequent screening of redox-related genes revealed the essential role of nitric oxide, produced by *Nos2b*, in triggering MG cell-cycle re-entry after the retinal injury. Notably, we developed a sophisticated viral-based approach to achieve the *cxcl18b*-defined MG transitional state-specific knockout *nos2b* successfully and verified the requirement of transitional state-specific NO signaling in injury-induced MG proliferation. These findings provide novel cellular and molecular insights into this species-specific post-injury MG cell-cycle re-entry process, with potential implications for the development of regenerative medicine strategies.

Results

Single-cell transcriptome analysis reveals the landscape of injury-induced Müller glia states

Zebrafish Müller glia can respond to retina injury by the cell cycle re-entry, a critical step evolutionarily absent from their mammalian counterparts but essential for neuron regeneration**(Goldman, 2014; Powell et al., 2016)**. We created a zebrafish retina injury model by crossing *Tg(opn1lws2: nfsb-mCherry)*^{uom3} (referred to as *Tg(lws2: nfsb-mCherry)*) with *Tg(mpeg1: GFP)* fish, in which the bacterial nitroreductase (NTR) enzyme was specifically expressed in G/R cone. We selectively

115 ablated the G/R cone starting at 5 days post-fertilization (dpf) by a subsequent 120
116 hours of metronidazole (MTZ) exposure**(Curado et al., 2007; Curado et al., 2008)**
117 **(Figure 1A and Figure 1-figure supplement 1A)**. G/R cone became significantly
118 reduced in number since 48 hours post-injury (hpi) and was mostly depleted at 120
119 hpi **(Figure 1B)**. Meanwhile, a number of microglia (marked by *Tg(mpeg1: GFP)*)
120 migrated to the outer nuclear layer (ONL) as early as 48 hpi, peaked at 72 hpi, and
121 began to reduce in number at 96 hpi and onward **(Figure 1C)**. Notably, in response to
122 G/R cone ablation, the proliferative MG population increased starting at 48 hpi,
123 peaked at 72 hpi, and began to decline since 96 hpi and forward **(Figure 1D)**. In light
124 of the result that the number of proliferative MG peaked at 72 hpi, we focused on the
125 72-hpi time point for the further exploration of MG proliferative behaviors following
126 G/R cone ablation **(Figure 1E)**.

127 By revisiting previously obtained scRNA-seq data of MG enriched from
128 *Tg(lws2: nfsb-mCherry)* crossed with *Tg(gfap: EGFP)* and *Tg(her4.1: dRFP)* retina
129 before and after G/R cone ablation at 72 hpi**(Krylov et al., 2023)**, we selected 5,932
130 and 3,999 MG cells and their derived progenies from the uninjured and 72-hpi retina,
131 respectively **(Details in Methods; Figure 1-figure supplement 1B)**. By clustering
132 these cells, we identified 13 clusters, 8 out of which (Clusters 2, 3, 5, 6, 9, 10, 11, and
133 12) with an increased proportion in response to the G/R cone ablation **(Figure 1-**
134 **figure supplement 1C)**. Subsequently, we re-clustered cells of these 8 clusters (695
135 cells of uninjured retinae and 3,477 cells of 72-hpi retinae), aggregating into 10 new
136 clusters. After the quality control procedure, we did not consider Clusters 7/8/9 due to

137 their small populations with ribosomal, dendritic, and doublet features, resulting in 7
138 clusters for further analysis. (Details in Methods; **Figure 1F)**

139 We performed the pseudo-time trajectory analysis to reveal the progression of
140 these MG clusters following the cone ablation **(Figure 1G)**. Cluster 4 cells were
141 highly expressing genes related to mature MG (*glula*, *slc1a2b*, *apoeb,* and
142 *rlbp1a*)**(Bernardos and Raymond, 2006; Raymond et al., 2006; Thummel et al.,**
143 **2008; Yurco and Cameron, 2005)**, the quiescent state (*cx43*)**(Dermietzel et al.,**
144 **2000; Janssen-Bienhold et al., 1998)** and major MG population marker
145 (*fgf24*)**(Krylov et al., 2023) (Figure 1-figure supplement 1D)**. Furthermore, Cluster
146 4 began to express *s100α10b* and *gfap,* reactive state makers**(Celotto et al., 2023;**
147 **Hoang et al., 2020)**, in the injured retinae, but not in the uninjured retina **(Figure 1-**
148 **figure supplement 1D)**. Thus, we set Cluster 4 as the most original MG states.

149 To examine the transition of these 7 MG clusters, the pseudo-time trajectory
150 showed that the main developmental branch consisted of Clusters 4/1/2 and then
151 became divergent into two sub-branches, including Cluster 0 and 5/3/6 (**Figure 1G)**.
152 In contrast to the sub-branch of Cluster 0, the sub-branch of Clusters 5/3/6 was highly
153 expressing proliferative cell markers (*pcna, mki67,* and *mcm2*). Within the latter sub-
154 branch, while Cluster 3 and 6 with the highest levels of proliferative cell markers,
155 Cluster 6 began to express neuronal differentiation factors (*otx5, crx,* and
156 *pde6gb*)**(Abalo et al., 2020; Asaoka et al., 2014; Shen and Raymond, 2004)**
157 **(Figure 1-figure supplement 1D)**. Thus, we identified 6 major post-injury MG states,
158 from the most original states (Cluster 4) to three transitional states (Cluster 1/2/5), to

159 finally two proliferative states (Cluster 3/6).

160 Remarkably, chemokine (C-X-C motif) ligand 18b *(cxcl18b*), an inflammatory
161 chemokine, was uniquely expressed in three transitional states but largely absent from
162 the most original Cluster 4 and two proliferative Cluster 3/6. Specifically, while the
163 first *cxcl18b*$^{+}$ transitional state (Cluster 1) was expressing *cx43*, a maker for MG
164 quiescence**(Dermietzel et al., 2000; Janssen-Bienhold et al., 1998)**, the last
165 transitional state (Cluster 5) began to show a weak induction of *ascl1α*, a master
166 regulator of injury-induced MG reprogramming**(Ramachandran et al., 2010)**.
167 Immediately following this last transitional state, Cluster 3 started with high *ascl1α*
168 expression and entered the proliferative state with the expression of *pcna* and *mik67*
169 **(Figure 1H)**. Our analysis highlighted a new set of *cxcl18b*-defined MG transitional
170 states preceding *ascl1α* induction, bridging MG from the most original quiescence
171 state to injury-induced proliferation.

172

173 **Clonal analysis revealing injury-induced MG proliferation via inflammation**
174 **inducted *cxcl18b*-defined transitional states**

175 To directly verify the presence of *cxcl18b*-defined MG transitional states, we first
176 examined the temporal relationship of *cxcl18b* expression and MG proliferation after
177 the cone ablation using *in situ* hybridization combined with immunostaining of either
178 BLBP (an MG maker) or PCNA (a proliferative cell maker) **(Figure 2A and Figure**
179 **2-figure supplement 1A)**. The result showed that as early as 24 hpi, the number of
180 *cxcl18b*$^{+}$ MG was rapidly peaked with no emergence of proliferative MG **(cell**

181 **number: 11 ± 4, n=10 in *cxcl18b*$^+$ MG; mean ± SEM)**, and then *cxcl18b*$^+$ MG
182 continued declining in number over time and reached the lowest level since 96 hpi **(1**
183 **± 1, n=7; mean ± SEM; Figure 2B)**. In contrast, the number of proliferative MG
184 (PCNA$^+$) peaked at 72 hpi and decreased to the lowest level at 120 hpi **(9 ± 2, n=11 in**
185 **72-hpi retina; 1 ± 1, n=5 in 120-hpi retina; mean ± SEM; Figure 2B)**. Note that
186 *cxcl18b*$^+$ MG was mostly proliferative at 72 hpi **(Figure 2-figure supplement 1B)**.
187 To further verify the temporal expression of *cxcl18b* in MG following the cone
188 ablation, we created a new transgenic reporter *Tg(cxcl18b: GFP)* by cloning a 3k-bp-
189 long cis-element of 5'UTR with GFP, allowing real-time monitoring of injury-induced
190 *cxcl18b* expression *in vivo* **(Figure 2C and Figure 2-figure supplement 1C-D)**.
191 Combining this line with PCNA immunostaining, we confirmed the remarkable
192 increase of *cxcl18b* expression (GFP$^+$) at 48 hpi **(0 ± 1, n=4 in uninjured retinas vs**
193 **11 ± 4, n=7 in 48-hpi; mean ± SEM; Figure 2D and E)**. Due to the prolonged stay
194 of GFP protein, we could also observe some GFP$^+$ MG has become proliferative
195 (PCNA positive) **(Figure 2D)**. The result of proliferative MG as a subpopulation of
196 *cxcl18b*$^+$ MG led to an outstanding question as to whether *cxcl18b*-defined MG
197 transitional states represented an essential route to injury-induced proliferation.
198 To address it, we created a new transgene *Tg(cxcl18b: Cre-vmhc: mCherry::*
199 *ef1α: loxP-DsRed-loxP-EGFP:: lws2: nfsb-mCherry)* to perform the clonal analysis
200 of *cxcl18b*-expressing MG after the G/R cone ablation **(Details in Method; Figure 2-**
201 **figure supplement 1E)**. After ablating the G/R cone by MTZ treatment at 6 dpf for 3
202 consecutive days, we found that the numbers of *cxcl18b*$^+$ MG and PCNA$^+$ MG were

203 significantly increased at 72 hpi **(Figure 2F)**. Further analysis showed that all PCNA$^+$
204 MG were *cxcl18b*$^+$, indicating the *cxcl18b*$^+$ MG were the ones who could eventually
205 enter into the cell cycle **(13 ± 2 cells for PCNA$^+$ vs 13 ± 2 cells PCNA$^+$ and**
206 ***cxcl18b*$^+$ MG; percentage of PCNA$^+$ and *cxcl18b*$^+$ vs PCNA$^+$ = 93 ± 2%; n=14;**
207 **p=0.19; Mean ± SEM; Figure 2G)**. Further analysis showed that at 120 hpi, the time
208 point that the MG proliferation has largely creased, GFP$^+$ MG with the lineage history
209 of injury-induced *cxcl18b* expression constituted about 44% of GS$^+$ MG at the central
210 retina, indicating that only about half of MG could enter *cxcl18b*$^+$ transitional states
211 following the cone ablation **(cell number of clones: 14 ± 3 in GS$^+$ and Cre$^+$ MG; 28**
212 **± 4 in GS$^+$ and Cre$^-$ MG, n=14; p<0.05; mean ± SEM; Figure 2I)**. Together, our
213 clonal analysis demonstrated that proliferative MG mostly originated from *cxcl18b*$^+$
214 MG transitional states, and 44% central MG could become *cxcl18b* positive. To
215 investigate whether *cxcl18b* was required for MG proliferation following G/R cone
216 ablation, we employed CRISPR-Cas9-mediated gene disruption, using two sgRNAs
217 targeting *cxcl18b* **(Figure 2-figure supplement 1F and G)**. We found that *cxcl18b*
218 knockout did not reduce MG proliferation after G/R cone ablation at 72 hpi (**13 ± 3,**
219 **n=11 in WT; 11 ± 3, n=7 in *scramble* sgRNA-injected; 13 ± 3, n=7 in *cxcl18b***
220 **sgRNA-injected; mean ± SEM**), suggesting that *cxcl18b* per se does not regulate
221 MG proliferation directly **(Figure 2-figure supplement 1H and I)**. This led us to
222 wonder about the induction of *cxcl18b*-defined MG transitional states.

223 As an inflammatory chemokine, *cxcl18b* serves as a reliable marker of
224 inflammation and regulates neutrophil recruitment to injury sites**(Goumenaki et al.,**

225 **2024; Torraca et al., 2017)**. Inflammation has been previously shown to be critical
226 for inducing regenerative responses in adult zebrafish, where it promotes reactive
227 microglia/macrophages and Müller glial proliferation in the retina**(Iribarne and**
228 **Hyde, 2022; Kyritsis et al., 2012)**. Notably, suppressing the immune response using
229 dexamethasone (Dex) in zebrafish retina reduced microglial reactivation and
230 significantly decreased the number of proliferative MG**(Silva et al., 2020; Zhang et**
231 **al., 2020)**. In our study, we identified the *cxcl18b*-defined transitional states as the
232 essential routing for MG proliferation after G/R cone ablation. These results prompted
233 us to investigate whether the inflammatory responses mediated by recruited microglia
234 are indispensable for the formation of these *cxcl18b*-defined transitional states.

235 To address this, we examined *cxcl18b* expression using *Tg(cxcl18b: GFP)* after
236 inhibiting inflammation using Dex**(Iribarne and Hyde, 2022)**, and observed a
237 significant reduction in the number of *cxcl18b*$^{+}$ MG (GFP^{+} cells) at 72 hpi **(11 ± 4,**
238 **n=10 in Dex treated retina vs 19 ± 5, n=6 in DMSO treatment; and 18 ± 3, n=14**
239 **in the 72-hpi retina; mean ± SEM) (Figure 2K)**. Consistent with earlier reports, we
240 observed that Dex treatment inhibited the migration of microglia **(indicated by**
241 ***Tg(mpeg1: GFP)*; 16 ± 4, n=14 in Dex treated retina vs 27 ± 5, n=7 in DMSO**
242 **treatment; and 28 ± 4, n=9 in the 72-hpi retina; mean ± SEM)** to the ONL and
243 significantly reduced the number of proliferative MG **(PCNA^{+}; 8 ± 2, n=14 in Dex**
244 **treated retina vs 17 ± 2, n=7 in DMSO treatment; and 14 ± 3, n=9 in the 72-hpi**
245 **retina; mean ± SEM)** at 72 hpi after G/R cone ablation **(Figure 2L and M and**
246 **Figure 2-figure supplement 1J)**. These findings strongly suggested that injury-

247 induced, microglia-mediated inflammation is critical for activating the *cxcl18b*-
248 defined transitional states that drive MG proliferation.
249
250 ***cxcl18b*-defined MG transitional states recapitulate molecular features of retinal**
251 **stem cells in the ciliary marginal zone**
252 Interestingly, we observed the *cxcl18b* expression in the CMZ after the cone
253 ablation besides its high expression in the MG **(Figure 2A)**. We were then curious
254 about the *cxcl18b* expression in the developmental retina as well as in the CMZ
255 without the injury. Notably, *in situ* results showed that *cxcl18b* was largely absent
256 from the central region but presented in the peripheral region of 30-hpf retinae,
257 whereas it was highly expressed in the most peripheral region of the CMZ, where
258 *fabp11a* and *col15α1b*, two putative makers for post-embryonic retinal stem cells
259 (RSCs) are located**(Gonzalez-Nunez et al., 2010; Raymond et al., 2006) (Figure**
260 **3A-B and E-F, and Figure 3-figure supplement 1A)**. The transgenic line of
261 *Tg(cxcl18b: GFP)* also showed a robust *cxcl18b* expression in the CMZ **(Figure 3-**
262 **figure supplement 1D)**. Consistently, our scRNAseq data of CMZ cells also
263 confirmed the co-expression of *cxcl18b*, *fabp11a*, and *col15α1b* **(Figure 3C-D and**
264 **G-H, and Figure 3-figure supplement 1B)**. Furthermore, cluster 1 MG, at the earlier
265 stage of transitional states, has the highest *cxcl18b* expression with *col15α1b*
266 expression **(Figure 1F and Figure 3-figure supplement 1C)**. All these results
267 suggested that *cxcl18b*-defined transitional states, at least to some extent, represent
268 the developmental state of retinal stem cells in the CMZ, but not that of embryonic

269 retinal progenitors.

270

271 ***Nos2b* is required for MG entry into the proliferation via NO signaling**

272 Previous studies have demonstrated the involvement of redox signaling in cell
273 regeneration processes in various tissues across species**(Han et al., 2014; Hunter et**
274 **al., 2018; Matrone et al., 2021; Yoo et al., 2012)**. All these evidences led us to
275 directly test the roles of redox genes in serving as the molecular mechanism
276 underlying injury-induced MG proliferation. Thus, we first examined the expression
277 levels of a comprehensive list of redox genes in *cxcl18b*-defined MG transitional
278 states (Clusters 1/2/5) in our scRNA-seq data **(Figure 1H)** and screened the influence
279 of 18 genes from each major category of redox signaling on injury-induced MG
280 proliferation using CRISPR-Cas9-mediated gene disruption **(Figure 4-figure**
281 **supplement 1A)**. We focused on the nitric oxide (NO) signaling pathway, targeting
282 three genes encoding nitric oxide synthases (*Nos*): neuronal *Nos* (*nos1*) and two
283 inducible forms (*nos2a* and *nos2b*), as well as the gene encoding S-nitrosoglutathione
284 reductase (*gsnor* or *adh5*), which modulates reactive NO signaling **(Figure 4A and**
285 **Figure 4-figure supplement 1B)**. The consequence and efficiency of gene disruption
286 were verified by DNA sequencing **(Figure 4-figure supplement 1C)**. Notably, the
287 disruption of *nos2b* resulted in a significant reduction of $PCNA^+$ MG at 72 hpi
288 **(number of $PCNA^+$ clones: 6±2, n=22 in *nos2b*-disrupted vs 11±3, n=7 in**
289 ***scramble* sgRNA-injected; Mean ± SEM) (Figure 4B)**. Noted that *nos* gene
290 disruption did not significantly alter microglia recruitment or G/R cone ablation at 72

291 hpi, suggesting that the influence of NO on injury-induced MG proliferation was not
292 via inflammatory reactions of recruited microglia or injury degree **(Figure 4-figure**
293 **supplement 1D-F)**.

294 To further examine the function of *Nos2b* via NO, we employed various *Nos*
295 inhibitors (L-NG-nitro arginine methyl ester, L_NAME; L-NG-Monomethyl
296 Arginine, L_NMMA; 1400W) and NO scavengers (carboxy-PTIO, C-
297 PTIO)**(Goldstein et al., 2003; Hong et al., 2012; Moore et al., 1990; Rees et al.,**
298 **1990)**. We performed the intravitreal injection of the drugs (PBS as control) into the
299 zebrafish eye from 2 days before cell ablation until 72 hpi **(Figure 4C)**. Notably, the
300 NO scavenger C-PTIO mostly suppressed MG proliferation, indicating the
301 involvement of NO **(cell number of PCNA^{+} MG: 3±2, n=27 after blocking NO by**
302 **C-PTIO vs 14±4, n=16 in PBS-injected retina; Mean ± SEM) (Figure 4D and E)**.
303 Moreover, 1400W (an inhibitor specific to inducible *Nos*, **7±2, n=10; Mean ± SEM**)
304 and L_NAME (a broad inhibitor to all three *Nos* forms, **8±2, n=12; Mean ± SEM**)
305 could also significantly reduce the number of proliferative MG after the ablation,
306 whereas L_NMMA (the inhibitor specific to neuronal *Nos*) did not influence MG
307 proliferation (**11±3, n=12; Mean ± SEM**) **(Figure 4E)**. Taken together, these results
308 highlight the critical role of NO signaling in regulating injury-induced MG
309 proliferation.

310 We further generated nitric oxide pathway mutant zebrafish (*nos1*, *nos2a*, *nos2b*,
311 and *gsnor*) to investigate the role of NO in MG proliferation following G/R cone
312 ablation. Utilizing CRISPR/Cas9-mediated gene disruption, we successfully screened

313 out *nos1*, *nos2a*, *nos2b*, and *gsnor* mutants, characterized by deletions of 133-bp, 13-
314 bp, 220-bp, and 11-bp coding sequences, respectively (see Methods for details,
315 **Figure 4-figure supplement 2A and B)**. Consistent with the gene disruption
316 experiment above, in both heterozygous and homozygous, we observed a significant
317 reduction in proliferative ($PCNA^+$) MG at 72 hpi following G/R cone ablation in
318 *nos2b* mutant **(3±1, n=20 in *nos2b*$^{+/-}$ mutants and 6±2, n=20 in *nos2b*$^{-/-}$, vs 11±2,**
319 **n=14 in WT; Mean ± SEM)**, while no influenced across the *nos* mutants (*nos1*,
320 *nos2a*) and *gsnor* mutants **(Figures 4F-4I)**.

321 Interestingly, the reduction in proliferative MG was more pronounced in *nos2b*
322 heterozygous mutants (*nos2b*$^{+/-}$) than in homozygous mutants (*nos2b*$^{-/-}$) **(*nos2b*$^{+/-}$ vs**
323 ***nos2b*$^{-/-}$; p<0.001; Mean ± SEM) (Figure 4J)**. We observed that cone ablation
324 induced by injury was not significant in *nos2b* mutants, indicating that the observed
325 differences in MG proliferation regulated by NO in these mutants are independent of
326 the injury **(45±8 photoreceptor cells remain, n=24 in WT; vs 49±12, n=20 in**
327 ***nos2b*$^{+/-}$ mutants and 46±9, n=20 in *nos2b*$^{-/-}$; Mean ± SEM) (Figure 4K)**. This
328 unexpected result suggests a concentration-dependent effect of NO on proliferative
329 MG. Specifically, compared to homozygous mutants, heterozygous mutants with
330 intermediate NO levels more effectively suppressed MG proliferation, whereas wild-
331 type animals with higher NO levels promoted MG proliferation. This concentration-
332 response pattern highlights the role of NO as a regulator, rather than a mediator, of
333 injury-induced MG proliferation.

334

335 **Specific *nos2b* expression in *cxcl18b*-defined transitional states MG after G/R**
336 **cone ablation**

337 To further examine whether the expression of *nos2b* in *cxcl18b*$^+$ MG, we used
338 the newly generated transgene fish line in our study *Tg(cxcl18b: GFP)*, enabling us to
339 monitor *cxcl18b*$^+$ MG after the G/R cone ablation in a real-time manner. By crossing
340 different fish lines, we fluorescently sorted out three post-injury MG populations (72-
341 hpi MG, 72-hpi PCNA$^+$ MG, and 72-hpi *cxcl18b*$^+$ MG) and three control groups
342 (uninjured MG, 72-hpi retinal cells other than MG and 72-hpi G/R cone) **(Figure 5A-**
343 **C)**. The real-time quantitative PCR (RT-qPCR) analysis showed that compared to the
344 three control groups, the expression of *nos2b* was significantly higher in *cxcl18b*$^+$ MG
345 than in 72-hpi MG and 72-hpi PCNA$^+$ MG **(relative expression of *nos2b*: 89±32,**
346 **repeats n=7 in *cxcl18b*$^+$ MG; 14±17, repeats n=5 in 72-hpi MG; and 1±1, repeats**
347 **n=6 in PCNA$^+$ MG; Mean ± SEM) (Figure 5D and Figure 5-figure supplement**
348 **1D-F)**. Together with the fact that *cxcl18b*$^+$ MG contained PCNA$^+$ and PCNA$^-$
349 populations in *Tg(cxcl18b: GFP)* **(Figure 2D)**, our result indicated that *nos2b* was
350 specifically expressed in *cxcl18b*$^+$ non-proliferative MG, which was in agreement
351 with the scRNA-seq result of the specific expression of *cxcl18b* in three transitional
352 states (Clusters 1, 2, and 5; **Figure 1H**). *In situ* hybridization using an HCR molecular
353 probe in the *Tg(lws2: nfsb-mCherry* x *cxcl18b: GFP)* fish line also suggests that
354 injury-induced *nos2b* expression was specific in the *cxcl18b*-defined transitional state
355 MG **(Figure 5-figure supplement 1A-C)**. Thus, our analysis reveals that *nos2b* was
356 specifically expressed in *cxcl18b*$^+$ transitional MG states, particularly in non-

357 proliferative cells.

358

359 **NO produced by *nos2b* determines *cxcl18b*$^+$ MG entry for proliferation**

360 To further explore the role of *cxcl18b*$^+$ MG-specific *nos2b* in regulating the entry
361 of MG proliferation after the G/R cone ablation, we developed a sophisticated clonal
362 analysis of *cxcl18b*$^+$ MG with genetic disruption of *nos2b* using CRISPR-Cas9
363 method. To achieve glial type-specific gene manipulation, we employed an
364 adenovirus strain that specifically infects radial glia in zebrafish**(Jia et al., 2019; Liu**
365 **et al., 2021)**, and confirmed that it could faithfully mark MG in the zebrafish retina
366 **(Figure 6A and B)**. For the clonal analysis, we performed the intravitreal injection of
367 two viruses packaged with elements of *cxcl18b: gal4* and *UAS: Cas9-T2A-Cre-u6:*
368 *sgRNA (nos2b)* into the eye of *Tg(lws2: nfsb-mCherry,ef1α: loxP-DsRed-loxP-EGFP)*
369 at 5 dpf, virus packaged with element of *UAS: Cas9-T2A-Cre-u6: empty* as the control
370 **(Figure 6C-D and Figure 6-figure supplement 1A)**. One day after the virus
371 infection, the fish was treated with MTZ for 3 consecutive days to ablate the G/R cone
372 **(Figure 6E)**.

373 At 72 hpi, we collected the clones (GFP$^+$) derived from *cxcl18b*$^+$ MG and
374 analyzed their proliferative property **(Figure 6F and G)**. The analysis of virus-
375 infected clones (GFP$^+$) cell cycle re-entering (PCNA$^+$) after G/R cone ablation
376 revealed that only ~23% of GFP$^+$ MG clones remained PCNA$^+$ in the *nos2b* knockout
377 group, compared to ~75% in the control group **(Figure 6H)**. Note that the efficiency
378 of *nos2b* sgRNAs was confirmed in terms of mutation types and knockout efficiency

379 by sequencing **(Figure 6-figure supplement 1B-D)**.

380 Taken together, these findings suggested that it is the NO produced by *Nos2b*
381 within *cxcl18b*-defined transitional state MG that specifically drives MG from the
382 transitional state into proliferation following injury, highlighting a pivotal mechanism
383 underlying injury-induced regenerative processes.

384

385 **NO decreased Notch activity that is responsible for injury-induced MG**
386 **proliferation**

387 Previous studies have shown that *ascl1α* and Notch signaling are essential for
388 MG proliferation in the injured zebrafish retina**(Conner et al., 2014; Wan et al.,**
389 **2012)**. Regarding Notch signaling, a high Notch3 expression is reported to maintain
390 MG quiescence. In response to the injury, *notch3* expression is downregulated, but
391 *notch1a* is necessary for the continued proliferation of the progenitors**(Campbell et**
392 **al., 2022)**. In consistent, we observed that *notch3* and *hey* (the Notch downstream
393 target) were highly expressed in uninjured MG clusters and became reduced from the
394 most original states (Cluster4) to the proliferative states **(**Cluster 3 and 6**)**, whereas
395 *notch1a/1b* and *ascl1α* were prominently expressed in the late stage of *cxcl18b*$^{+}$
396 transitional states (clusters 5) and the proliferative states **(**Cluster 3; **Figure 1H and**
397 **7A)**. Interestingly, upstream regulators of Notch signaling activation, such as *fgf8a*,
398 *fgf8b***(Wan and Goldman, 2017)**, and *tgfb3***(Lee et al., 2020)**, were predominantly
399 expressed in clusters 4 and 1, preceding the expression of *cxcl18b* **(Figure 7A)**. These
400 results led us to wonder whether NO regulated *cxcl18b*-defined transitional state MG

401 cell cycle re-entry via the Notch signaling pathway.

402 To examine the influence of NO signaling blockage on Notch activity dynamics
403 following the cone ablation, we employed a reporter line *Tg(Tp1bglob: EGFP)*
404 (referred to as *Tg(Tp1:EGFP)*), in which EGFP is driven by the TP1 element, the
405 direct target of the intracellular domain of Notch receptors (NICD) that is generated
406 upon Notch activation**(Parsons et al., 2009; Quillien et al., 2014)**. We treated fish
407 with the NO scavenger C-PTIO and MTZ, starting at 5 dpf for 5 continuous days and
408 at 7 dpf for 3 continuous days, respectively, followed by immunostaining for EGFP
409 and PCNA **(Figure 7B)**. Interestingly, *Tp1*: $EGFP^+$ MG were significantly reduced at
410 all three injury time points **(cell number of $EGFP^+$ clones: 34±3, n=9 in 24-hpi**
411 **retina; 29±3, n=4 in 48-hpi retina; 33±4, n=6 in 72-hpi retina vs 42±1, n=4 in the**
412 **uninjured retina; Mean ± SEM)**, demonstrating a decrease in Notch activity
413 following G/R cone ablation **(Figure 7C)**. Notably, this reduction in Notch activation
414 was further rescued by NO blocking using C-PTIO (**cell number of $EGFP^+$ clones:**
415 **42±1, n=6 in C-PTIO treated retina at 24 hpi; 42±2, n=5 at 48 hpi; 44±2, n=7 at**
416 **72hpi; Mean ± SEM**), suggesting that NO modulates Notch signaling **(Figure 7C)**.
417 Meanwhile, C-PTIO treatment significantly reduced the number of proliferative MG
418 (marked by PCNA) **(Figure 7D)**. These findings indicated that injury-induced NO
419 suppresses Notch signaling activation, which potentially drives MG to exit quiescence
420 and enter proliferation. Together, our results highlight that NO signaling drove the
421 injury-induced *cxcl18b*-defined transitional state MG to enter into proliferation, which
422 may be mediated by Notch pathway regulation.

Discussion:

Our study provides the single-cell transcriptomic landscape of Müller glia (MG) state progression following the cone ablation. Combined with clonal analysis, we identified a previously unreported *cxcl18b*-defined transitional MG state as the essential routing for MG cell cycle re-entry. It led to our further genetic analysis revealing the concentration-dependent regulatory mechanism of nitric oxide derived from *nos2b* underlying injury-induced MG proliferation. Furthermore, NO signaling accounted for a decreased Notch activity, which has been previously reported to be essential for MG proliferation after the injury. Finally, cell state-specific gene disruption revealed that *cxcl18b*-defined MG transitional state-specific *nos2b* is required for injury-induced MG proliferation. Thus, our study provides the novel redox-related mechanism underlying MG proliferation in response to cone ablation in the zebrafish retina, opening up exciting possibilities for future research and potential therapeutic interventions.

Identification of *cxcl18b*-defined MG transitional states following the cone ablation

Combined scRNA-seq analysis and clonal analysis, we identified a previously unreported transitional MG state, marked by the expression of *cxcl18b,* as the essential routing for MG to re-enter the cell cycle following the retina injury **(Figure 1H, 2F, and 2G)**. To our knowledge, it is the first transitional state verified by *in vivo* clonal analysis to show a faithful prediction of injury-induced MG proliferation. Notably, this *cxcl18b* induction in MG depends on microglial recruitment in response to cone ablation, suggesting this transitional state is an MG response to the signals derived from the inflammatory reaction **(Figure 2K)**. The underlying mechanism of this crosstalk is crucial to be addressed. Interestingly, the *cxcl18b*-containing gene module was also expressed in the CMZ, a region crucial for adult retina neurogenesis for a lifetime **(Figure 3A-D)**. However, its expression is mainly absent from the central regions of the developing retina **(Figure 3F)**. It suggests that the *cxcl18b*-defined transitional state might represent a developmental state used by constitutive

neuron generation programs and injury-induced neuron regeneration programs beyond embryonic development. Furthermore, the *cxcl18b*-defined transitional state exhibits robust redox-related characteristics, such as the expression of *sod1*, *sod2*, and *catalase* **(Figure 4-figure supplement 1A)**. It led to the critical discovery of this study, which showed the essential role of *nos2b* in regulating injury-induced MG proliferation. Unfortunately, our preliminary effects on gene disruption using CRISPR/Cas9 in F0 founders did not observe a significant reduction in the number of proliferative MG after *cxcl18b* disruption **(Figure 2-figure supplement 1I)**. However, a recent study reported the essential role of *cxcl18b* in heart regeneration using mutant fish, providing a mechanism of *cxcl18b* as innate immune signaling in injury-induced tissue regeneration**(Goumenaki et al., 2024)**. Their results raised concern about the efficiency of *cxcl18b* disruption in our system. It is essential to use mutant fish to re-examine the role of *cxcl18b* in injury-induced MG proliferation in the future. Also, we cannot rule out the possibility that other co-factors are involved in the action of *cxcl18b* in MG regeneration, which is another critical issue that needs to be solved in the future.

The possible mechanism of NO signaling underlying injury-induced MG proliferation

Our study, for the first time, demonstrated an essential role of NO signaling in regulating MG proliferation after the cone ablation. However, we still need to understand more about the underlying mechanism. There are two well-characterized molecular events responsible for MG proliferation following the retina injury: a decreased Notch activity and an increased *ascl1α* expression**(Fausett et al., 2008; Jorstad et al., 2017; Ramachandran et al., 2010)**. Previous studies have shown that Notch3 is responsible for this decreased Notch activity, leading to increased Ascl1a through the de-depression mechanism**(Campbell et al., 2021; Sahu et al., 2021).** Interestingly, unlike *notch3*, *notch1a* has been reported to stimulate MG proliferation**(Campbell et al., 2021; Campbell et al., 2022)**. Our scRNA-seq analysis also showed that as MG progressed into the proliferative states after the cone ablation,

notch3 expression gradually declined **(Figure 7A)**. In contrast, *ascl1α, notch1a, and notch1b* expressions were up-regulated and peaked at the proliferative states **(Figure 7A)**. Thus, both previous studies and our current analysis support the idea that the transcriptional regulation of Notch expression accounts for the decreased Notch activity after the injury. Intriguingly, NO has been reported to activate the Notch1 signaling cascade by promoting the release and accumulation of the Notch1 intracellular domain (NICD) through nitrification reactions, subsequently enhancing tumorigenesis and stem-like features in various cellular systems**(Charles et al., 2010; López-Juárez et al., 2017; Villegas et al., 2018)**. It raises the possibility that NO signaling regulates injury-induced MG proliferation through the post-translational modification of Notch3. Previous studies have demonstrated two significant forms of NO-mediated post-modification: S-nitrosylation on cysteines and nitration on tyrosine. Our preliminary analysis showed that all 11 cysteine residues within the putative γ-secretase-dependent cleavage sites are conserved between Notch1a and Notch3, while notable differences were observed at four tyrosine residues. It leads to an outstanding question of whether NO regulated injury-induced MG proliferation by decreasing Notch activity via tyrosine nitration of Notch3, which is worthwhile to elucidate.

The production of NO signaling in MG following retina damage

Previous studies reported that *cxcl18b* is a reliable inflammatory marker**(Goumenaki et al., 2024; Torraca et al., 2017)** and different inflammation responses modulate MG proliferation in the damaged zebrafish retina**(Iribarne and Hyde, 2022)**. The induction of *cxcl18b* may represent the inflammatory responses of MG after the cone ablation, pointing out the potential link between the inflammatory response and the emergence of NO signaling in MG. Previous studies have demonstrated that iNOS is induced in various tissues by proinflammatory cytokines**(Förstermann and Sessa, 2012; Pacher et al., 2007)**. One of the approaches to test the role of inflammatory responses is to manipulate the levels of inflammatory responses in MG to see the NO production and MG proliferative

behaviors. Also, previous studies appreciate the essential role of electrical activity in tissue regeneration**(Levin, 2009; Qin et al., 2023)**; in particular, calcium signaling has been shown to regulate various molecular pathways for liver regeneration, including the hepatocyte growth factor-Met-tyrosine kinase (HGF-Met) transduction pathway(Bedi et al., 2024) and the epidermal growth factor receptor (EGFR) signaling(Kimura et al., 2023). It is interesting to speculate that the abnormal electrical activity of MG in the injured retina may result in an elevated level of intracellular calcium, which activates calmodulin and induces the conformation change of NOS to NO production**(Hanson et al., 2018; Jones et al., 2007)**. A similar mechanism has been proposed in the long-term potentiation of excitatory post-synaptic structure**(Grover and Teyler, 1990; Kawamoto et al., 2012; Park, 2018)** as well as in the glutamate neurotoxicity model**(Ashpole et al., 2013; Ashpole et al., 2012)**. Thus, the production of NO derived from *Nos* may be the product of the interplay between the inflammatory responses and the electrical activity in MG after the retina damage.

Limitations of this study

A few limitations of this study should be acknowledged: 1. The current study's description of the landscape of MG transitional states is based on single-cell transcriptomic data obtained at a single time point (72 hpi) after the cone ablation, which may not provide a complete picture of the state transition of post-injury MG. Future scRNA-seq analysis of MG at multiple post-injury time points is necessary to clarify this issue. 2. While we demonstrated a critical role of NO in injury-induced MG proliferation, the potential contribution of microglia-derived NO was not directly examined. 3. We did not perform direct measurements of NO levels specifically within *cxcl18b*-defined MG cells, leaving open the question of localized NO signaling.

Acknowledgments

This research was supported by grants from the National Key R&D Program of China (2022YFA1303000 to C.C.), the Chinese Academy of Sciences Strategic Priority Research Program B grants (XDB39000000 to C.C.), National Natural Science Foundation of China-Key program project (Grant No. 91849203 to C.C.), the Creative Research Groups of the National Natural Science Foundation of China (32321003 to J.H.), STI2030-Major Projects (2021ZD0204500 to J.H.), the National Key Research and Development Program of China (2020YFA0112700 to J.H.), National Natural Science Foundation of China (32471029 to J.H.).

Author Contributions

A.Y., design and experimental investigation, visualization, data analysis, methodology, writing-original draft, writing-review and editing. S.Y., M.D., and D.Z., investigation, methodology. J.H. and C.C., conceptualization, experimental design, data analysis, supervision, funding acquisition, writing-original draft, project administration, writing-review and editing.

Declaration of Interests

The authors declare no competing interests.

STAR METHODS

Detailed methods are provided in this version of this paper and include the following:

KEY RESOURCES TABLE
RESOURCE AVAILABILITY
Lead contact
Materials availability
Data and code availability
EXPERIMENTAL MODEL AND SUBJECT DETAILS
Single-cell RNA sequencing data analysis
Pseudo-time trajectory analysis
Zebrafish husbandry and transgenic fishlines
Generation of *Tg(cxcl18b: GFP)*
Generation of *Tg(cxcl18b: Cre-vmhc: mCherry:: ef1α: loxP-DsRed-loxP-EGFP:: lws2: nfsb-mCherry)*
Generation of mutant fish lines
Plasmid construction
Metronidazole treatment
Gene disruption via CRISPR/Cas9 system
Pharmacological Treatment with NO scavenger and dexamethasone or *Nos* Inhibitors intravitreal injection
The real-time quantitative PCR after FACS-sorted MG
Construction and injection of adenoviral-based MG-specific knockout system in the zebrafish retina
Tissue preparation and immunostaining
In situ hybridization
Imaging
Quantifications and statistical analysis

Key Resources Table

Key Resources Table				
Reagent type (species) or resource	**Designation**	**Source or reference**	**Identifiers**	**Additional information**
strain, strain background (Danio rerio)	Wild type	Dr William		AB
strain, strain background (Danio rerio)	*lws2: nfsb-mCherry*	Krylov et al., 2023		*Tg(opn1lws2: nfsb-mCherry)^{uom3}*
strain, strain background (Danio rerio)	*her4.1: dRFP*	Yeo et al., 2007	ZDB-TGCONSTRCT-070612–2	*Tg(her4.1: dRFP)*
strain, strain background (Danio rerio)	*gfap: EGFP*	Bernardos and Raymond, 2006	ZDB-FISH-150901–29307	*Tg(gfap: EGFP)*
strain, strain background (Danio rerio)	*mpeg1: GFP*	Ellett et al., 2011	ZDB-TGCONSTRCT-170801–5	*Tg(mpeg1: GFP)*
strain, strain background (Danio rerio)	*Tp1bglob: EGFP*	Yu and He, 2019		*Tg(Tp1bglob: EGFP)*
strain, strain background (Danio rerio)	*pcna: GFP*	Xu et al., 2020	ZDB-LAB-070129-2	*Tg(pcna: GFP)*
strain, strain background (Danio rerio)	*ef1α: loxP-DsRed-loxP-EGFP*	Hans et al., 2009		*Tg(ef1α: loxP-DsRed-loxP-EGFP)^{zf284}*
strain, strain background (Danio rerio)	*cxcl18b: Cre-vmhc: ECFP*	This manuscript		*Tg(cxcl18b: Cre-vmhc: ECFP; ef1α: loxP-DsRed-loxP-EGFP; lws2: nfsb-mCherry)*
strain, strain background (Danio rerio)	*cxcl18b: GFP*	This manuscript		*Tg(cxcl18b: GFP)*

antibody	Mouse monoclonal anti-PCNA	Abcam	Cat#Ab29; RRID: AB_303394	IF(1:500)
antibody	Rabbit polyclonal anti-BLBP	Abcam	Cat#ab32423; RRID: AB_880078	IF(1:1000)
antibody	Mouse monoclonal anti-Glutamine Synthetase	BD Biosciences	Cat# 610518; RRID: AB_397880	IF(1:1000)
antibody	Chicken monoclonal anti-GFP	Abcam	Cat# ab13970; RRID: AB_300798	IF(1:2000)
antibody	Rabbit polyclonal anti-GFPtag	Rabbit polyclonal anti-GFPtag	Cat#50430–2-AP; RRID: AB_11042881	IF(1:500)
antibody	Rabbit polyclonal anti-DsRed2	Takara Bio	Cat#632496; RRID: AB_10013483	IF(1:1000)
antibody	Alexa Fluor 488 AffiniPure Goat Anti-Mouse IgG (H+L)	Yeasen Biotech	Cat# 33206ES; RRID: AB_3662603	IF(1:1000)
antibody	Alexa Fluor 488 AffiniPure Donkey Anti-Rabbit IgG (H+L)	Yeasen Biotech	Cat# 34206ES60; RRID: AB_2909605	IF(1:1000)
antibody	Alexa Fluor 488 AffiniPure Donkey Anti-Chicken IgY (IgG) (H+L)	Jackson ImmunoResearch Labs	Cat# 703-545-155; RRID: AB_2340375	IF(1:1000)
antibody	Alexa Fluor 594 AffiniPure Donkey Anti-Mouse IgG (H+L)	Yeasen Biotech	Cat# 34112ES; RRID: AB_3661960	IF(1:1000)

antibody	Alexa Fluor 594 AffiniPure™ Goat Anti-Rabbit IgG (H+L)	Yeasen Biotech	Cat# 33112ES; RRID: AB_3661961	IF(1:1000)
antibody	Alexa Fluor 647-AffiniPure Goat Anti-Mouse IgG + IgM (H+L)	Jackson ImmunoResearch Labs	Cat# 115-605-044; RRID: AB_2338906	IF(1:1000)
recombinant DNA reagent	pTol2-cxcl18b: GFP	This manuscript		We made this plasmid by ligated the cxcl18b promoter and GFP element
recombinant DNA reagent	pTol2-cxcl18b: Cre-vmhc: mcherry	This manuscript		We made this plasmid by ligated the cxcl18b promoter and Cre element
recombinant DNA reagent	pTol2-cxcl18b: gal4FF	This manuscript		We made this plasmid by ligated the cxcl18b promoter and gal4FF element
recombinant DNA reagent	pUAS: Cas9T2ACre; U6: sgRNA1; U6: sgRNA2	Di Donato et al., 2016	Addgene plasmid #74010; RRID: Addgene_74010	
recombinant DNA reagent	pTol2-UAS: Cas9-T2A-Cre-U6: nos2b sgRNA1; U6: nos2b sgRNA2	This manuscript		We made this plasmid by insert two sgRNAs of *nos2b* in 10xUAS backbone
commercial assay or kit	MEGAscriptTM T7 High Yield Transcription Kit	Invitrogen	Cat# AM1334	
commercial assay or kit	ClonExpress MultiS One Step Cloning Kit	Vazyme	Cat# C113-02	

commercial assay or kit	DIG RNA labeling kit	Roche	Cat# 11277073910	
chemical compound, drug	N(ω)-nitro-L-arginine methyl ester	Sigma-Aldrich	Cat# N5751-1G	10 mM
chemical compound, drug	N(ω)-Methyl-L-arginine acetate salt	Sigma-Aldrich	Cat# M7033-5MG	10 mM
chemical compound, drug	1400W dihydrochloride	MedChemExpress	Cat# HY-18730	200 nM
chemical compound, drug	Phenyl-4,4,5,5-tetramethyl imidazoline-1-oxyl 3-oxide	Sigma-Aldrich	Cat# P5084-25MG	10 mM
chemical compound, drug	Dexamethasone	Sigma-Aldrich	Cat# D1756	10 mM
chemical compound, drug	Metronidazole	Sigma-Aldrich	Cat# M3761-100G	10 mM
software, algorithm	FV10-ASW 4.0 Viewer	Olympus	www.olympus-global.com	Analysis image
software, algorithm	GraphPad Prism V 9.0.0	GraphPad Software	www.graphpad.com	Data analysis
software, algorithm	Cell Ranger Single Cell Software Suite (v2.1.0)	10x genomics	https://support.10xgenomics.com	scRNA-seq data analysis
software, algorithm	RStudio	RStudio IDE	https://posit.co/	scRNA-seq data analysis
software, algorithm	R 4.4.1	R-project	https://www.r-project.org/	scRNA-seq data analysis

software, algorithm	Seurat	Satijalab	https://satijalab.org/seurat/	scRNA-seq data analysis

Resource availability

Lead contact

Further information and requests for resources and reagents should be directed to and will be fulfilled by the lead contact, Chang Chen (changchen@moon.ibp.ac.cn).

Materials availability

All unique reagents generated in this study will be made available from the contact. We may require a completed MTA if there is potential for commercial application.

Data and code availability

This paper does not report new raw scRNA-seq data and original code. Any additional information required to reanalyze the data reported in this paper is available from the lead contact upon request.

604 ## Experimental Model and Subject Details

605 **Single-cell RNA sequencing data analysis**

606 In this study, single-cell RNA sequencing (scRNA-seq) raw data of Müller glia
607 enriched after G/R cone ablation at 72 hpi are from**(Krylov et al., 2023)**, embryonic
608 RPCs at 24 hpf and postembryonic retinal stem cells (RSCs) at 14 dpf are from**(Xu et**
609 **al., 2020)**. We re-processed the single-cell FASTQ sequencing reads (Novogene) and
610 converted to digital gene expression matrices using the Cell Ranger software (version
611 3.1.0) provided by 10X Genomics after mapping to the zebrafish GRCz11 (Ensembl
612 release-96) genome assembly. An average of 47,545 mean reads per cell with 1,343
613 median genes per cell in no ablation control, 63,177 mean reads per cell with 1,556
614 median genes per cell in G/R cone ablation (lws2_72 hpi), 61,772 mean reads per cell
615 with 2,474 median genes per cell in the embryonic RPCs at 24 hpf, and 49,243 mean
616 reads per cell with 1,181 median genes per cell in the postembryonic retinal stem cells
617 (RSCs) at 14 dpf were obtained.

618 We then used the *cellranger aggr* (version 6.0,
619 https://support.10xgenomics.com/single-cell-gene-
620 expression/software/pipelines/latest/using/aggregate) to aggregate the *cellranger*
621 counts from the two datasets and normalize them to the same sequencing depth. The
622 feature barcode matrix was recalculated and analyzed on the combined data. This
623 resulted in a dataset of 19,706 aggregated cells, with 100% of the no ablation control
624 reads retained and 71.4% of the *lws2_3 dpi* reads retained. The aggregated matrix for
625 the no ablation control and lws2_72 hpi samples was loaded into the Seurat R package
626 (version 4.3.0, https://satijalab.org/seurat/). Cells with gene expression of more than
627 200 and less than 4000, lower than 5% mitochondrial content were filtered for further
628 analysis. The filtered data were normalized, scaled, and clustered using principal
629 component analysis (PCA) with a significance threshold of $p < 0.001$ (FindClusters,
630 resolution = 0.5), and a UMAP was computed using scanpy.tl. umap, resulting in 20
631 distinct clusters. MG clusters were identified by high expression of marker genes
632 including *rlbp1a*, *fabp7a*, *slc1a2b*, *glula*, *glulb*, *gfap*, and *her4.1*. Proliferative MG
633 clusters were identified from proliferative cell clusters by high expression of

proliferative cell markers including *pcna*, *mki67*, *gfap*, *her4.1*, and low expression of the CMZ markers including *fabp11a*, *col15α1b*, *fabp7b*, *rx2*. We further analyzed the MG and proliferative MG clusters to obtain 13 clusters, including no ablation control 5,932 cells and G/R cone ablation 72 hpi 3,999 cells in the UMAP plot **(Figure 1-figure supplement 1B)**. We compared the proportion of cell numbers in each cluster before and after injury and chose clusters with the high proportion of cell numbers in G/R cone ablation 72 hpi (clusters 2, 3, 5, 6, 9, 10, 11, 12, and 13) to further clustered into 10 clusters **(Figure 1-figure supplement 1C)**.

Single-cell RNA sequencing data of embryonic RPCs at 24 hpf and postembryonic RCSs at 14 dpf were generated into 10 and 11 clusters, respectively. Each cluster is identified by the cluster-specific marker gene and different development stage markers including *fabp11a*, *col15α1b*, *cxcl18b*, *her4.2*, *npm1a*, *her9*, *fabp7a*, *dla*, *atoh7*, *vsx1*, *mafba*, *otx5*, and *rem1* (**Figure 3A, 3C and Figure 3-figure supplement 1A and B**).

Pseudo-time trajectory analysis

After the UMAP cluster analysis of the single-cell data, trajectory analysis was performed to investigate the pseudo-time transcriptomic change of these ten clusters using the 'monocle 2' R package, which revealed three distinct states **(Figure 1G)**.

Zebrafish husbandry and transgenic fishlines

All experimental zebrafish embryos, larvae, and adults were produced, grown, and maintained at 28°C according to standard protocols. Embryos and larvae were kept in embryo medium (E3; 5 mM NaCl, 0.17 mM KCl, 0.33 mM $CaCl_2 \cdot 2H_2O$, 0.33 mM $MgSO_4 \bullet 7\ H_2O$, 1.3×10^{-5} % w/v methylene blue in RO water) at 28.5 °C, under a 14:10 light: dark cycle. Animal procedures performed in this study were approved by the Animal Use Committee of the Institute of Neuroscience, Chinese Academy of Sciences (NA-069-2023).

Published fish lines used in this study include the following: AB (Wild type, WT) and transgenic lines (Tg): *Tg(opn1lw2: NTR-mCherry)*^{uom3} (ZDB-ALT-201012-

2)**(Wang et al., 2020)** in this study named *Tg(lws2: nfsb-mCherry)*, *Tg(gfap: EGFP)*^{mi2001} (ZDB-FISH-150901–29307)**(Bernardos and Raymond, 2006)**, *Tg(her4.1: dRFP)* (ZDB-TGCONSTRCT-070612–2)**(Yeo et al., 2007)**, *Tg(mpeg1: GFP)* (ZDB-TGCONSTRCT-170801–5)**(Ellett et al., 2011)**, *Tg(pcna: GFP)* (ZDB-LAB-070129-2)**(Xu et al., 2020)**, *Tg(ef1α: loxP-DsRed-loxP-EGFP)***(Hans et al., 2009)**, *Tg(Tp1bglob: EGFP)***(Yu and He, 2019)**.

Newly generated transgenic fishline contained: *Tg(cxcl18b: GFP)*, *Tg(cxcl18b: Cre-vmhc: mCherry:: ef1α: loxP-DsRed-loxP-EGFP:: lws2: nfsb-mCherry)*, and mutants *nos1*$^{+/-}$, *nos2a*$^{+/-}$, *nos2b*$^{+/-}$, *gsnor*$^{+/-}$, *nos1*$^{-/-}$, *nos2a*$^{-/-}$, *nos2b*$^{-/-}$, *gsnor*$^{-/-}$.

Generation of *Tg(cxcl18b: GFP)*

The plasmid of *pTol2-cxcl18b: GFP* (10 ng/ μl) and *tol2* mRNA (50 ng/ μl) were co-injected into a wild-type embryo at the one-cell stage. Zebrafish embryos with green fluorescent were grown at the E3 medium according to standard protocol and selected as the founder (F0). The adult F0 fish crossed with the wild-type selected the fish with GFP^{+} offspring as F1. In this stable transgenic line, *cxcl18b*$^{+}$ cells expressed the fluorescent protein GFP and the full name of this line is *Tg(cxcl18b: GFP)*.

Generation of *Tg(cxcl18b: Cre-vmhc: mCherry:: ef1α: loxP-DsRed-loxP-EGFP:: lws2: nfsb-mCherry)*

The plasmid of *pTol2-cxcl18b: Cre-vmhc: mCherry* (10 ng/ μl) and *tol2* mRNA (50 ng/ μl) were co-injected into the embryo obtained from *Tg(lws2: nfsb-mCherry)* cross *Tg(ef1α: loxP-DsRed-loxP-EGFP)* at the one-cell stage. Zebrafish embryos were maintained at E3 medium according to standard protocol. Larvae with *mCherry* expression in the heart and eyes were selected and grown as the founder (F0) for further construction. The adult founder was crossed with wild-type (AB), considering the expression of *cxcl18b* during zebrafish development, larvae with mCherry and GFP double positive were selected and grown as the F1. In this zebrafish line, EGFP permanently marks all cells that have expressed *cxcl18b*, as well as their entire lineage of progeny. The full name of this line is *Tg(cxcl18b: Cre-vmhc: mCherry:: ef1α: loxP-DsRed-loxP-EGFP:: lws2: nfsb-mCherry)*.

Generation of mutant fish lines

The CRISPR/Cas9 system was employed to efficiently and precisely generate mutant zebrafish lines**(Wu et al., 2018)**. Two sgRNAs targeting gene coding sequences involved in nitric oxide metabolism signaling (nitric oxide synthase, *Nos*; and S-nitrosoglutathione reductase, GSNOR) were designed based on the zebrafish GRCz11 genome assembly.

Primers were designed approximately 200 bp from the sgRNA target sites for genotyping (sgRNAs and genotyping primers are listed in **Supplementary Table S1**). We mixed the two sgRNAs (100 ng/μl) for each target gene with Cas9 protein (400 ng/μl) and injected them into transgenic fishline *Tg(lws2: nfsb-mCherry)* embryos at the one-cell stage. Adult fish were crossed with wild-type, and offspring displaying *mCherry* expression in the eyes at 5 dpf were selected for further genotyping. Mutants were confirmed by sequencing, and the fish with open reading frame (ORF) shift were collected as heterozygous fish for further studies.

Plasmid construction

We cloned the *cxcl18b* regulatory element (3048 bp upstream of the start codon including the *5'UTR*) as the *cxcl18b* promoter from the zebrafish genomic DNA **(Figure 2C)**. The primers used for amplification were 5'-GCATTTGTCTCCTCATGCATTGACTAC-3' (forward primer) and 5'-TTGCTGCAAACTATATGTAGGAAATGCTG-3' (reversed primer). For constructing the plasmids *pTol2-cxcl18b: GFP*, *pTol2-cxcl18b: Cre-vmhc: mCherry*, and *pTol2-cxcl18b: gal4FF*, each DNA elements cassette was inserted into the *pDestTol2pA2* vector**(Kwan et al., 2007)**. The plasmid of *pUAS: Cas9T2AGFP; U6: sgRNA1; U6: sgRNA2* was kindly provided by Professor Filippo Del Bene.**(Di Donato et al., 2016)**. To prepare for plasmid *pTol2-UAS: Cas9-T2A-Cre-U6-empty* and *pTol2-UAS: Cas9-T2A-Cre-U6: nos2b sgRNA1; U6: nos2b sgRNA2*, the same two *nos2b* sgRNAs used to construct *nos2b* mutant fish were inserted into *pUAS: Cas9T2AGFP; U6: sgRNA1; U6: sgRNA2* plasmid, with the *GFP* element replaced by *Cr*e using

ClonExpressMultiS One Step Cloning Kit (Vazyme, C113-02). For the plasmid construction of the MG-specific knockout system based on recombinant adenoviral vectors, regulatory elements were inserted into adenoviral vectors *pAdc68-S* according to the standard protocol outlined by Jia et al.**(Jia et al., 2019)**. The final plasmids generated included, *pAdC68XY2-E1-CMV-GFP pAdC68XY2-E1-10xUAS: Cas9-2a-Cre-U6: sgRNA1(nos2b); U6: sgRNA2(nos2b), pAdC68XY2-E1-cxcl18b: gal4FF* and *pAdC68XY2-E1-10xUAS: Cas9-2a-Cre-U6: empty* as the control. Plasmid construction primer sequences are listed in **Supplementary Table S2**.

Metronidazole treatment

Zebrafish larvae were exposed to a 10 mM metronidazole (MTZ) solution (Sigma-Aldrich, M3761-100G) in standard fish water. For *Tg(lws2: nfsb-mCherry)* larvae processed for immunohistochemical analysis, MTZ treatment was initiated at 6 dpf to ablate green and red cones. Larvae were maintained in the MTZ solution at densities of fewer than 50 larvae per 50 mL petri dish and kept at 28.5°C. The MTZ solution was refreshed every 24 hours to ensure continuous cone ablation until fixation in 4% PFA, while control larvae were kept in standard fish water.

Gene disruption via CRISPR/Cas9 system

We used the CRISPR/Cas9 system for efficient gene disruption. Two sgRNAs were designed to target the coding sequences of genes involved in the nitric oxide signaling pathway (including *nos1*, *nos2a*, *nos2b*, *gsnor*) and *cxcl18b*. The sgRNAs were in vitro transcribed and purified using the LiCl precipitation approach (MEGAscript T7 Transcription Kit, Invitrogen, AM1334). A mixture of the two sgRNAs (in total 200 ng/μl) with Cas9 protein (400 ng/μl, Novoprotein, E365-01A) were co-injected into the embryo of *Tg(lws2: nfsb-mCherry)* at the one-cell stage. The efficiency of gene knockout for each sgRNA was validated, as presented in **Figure 4-figure supplement 1C**.

Pharmacological treatment with NO scavenger and dexamethasone or

Nos Inhibitors intravitreal injection

Zebrafish larvae at 6 dpf were anesthetized in 0.04% MS222 (Sigma, A5040) for 30 to 45 seconds. Inhibitor solutions of 2 μL were prepared as follows: 10 mM *N(ω)*-nitro-L-arginine methyl ester (L-NAME, Sigma-Aldrich, N5751-1G), a broad *Nos* inhibitor, diluted in sterile PBS from a 100 mM stock; 10 mM N(ω)-Methyl-L-arginine acetate salt (L-NMMA, Sigma-Aldrich, M7033-5MG), a specific inhibitor of *nNos*, diluted in sterile PBS from a 20 mM stock; and 200 nM 1400W dihydrochloride (SW1400, MedChemExpress, HY-18730), a specific inhibitor of *iNos*, diluted in sterile PBS from a 39.97 mM stock. PBS was used as the control. Each solution was loaded into glass capillaries prepared using a micropipette puller (Narishige, PC-10) and connected to a microinjector (Applied Scientific Instrumentation, MPPI-3). Intravitreal injections of the inhibitor solutions were administered to the zebrafish eyes starting 2 days before G/R cone ablation and continued until 72 hpi **(Figure 4C)**.

Additionally, zebrafish were pre-treated with 10 mM of the NO scavenger, Phenyl-4,4,5,5-tetramethyl imidazoline-1-oxyl 3-oxide (C-PTIO, Sigma-Aldrich, P5084-25MG), diluted in standard water (from a 100 mM stock), or dexamethasone (Dex, Sigma-Aldrich, D1756) which diluted in DMSO, starting 2 days before G/R cone ablation and continuing until 72 hpi **(Figure 2J and 4C)**.

The real-time quantitative PCR after FACS-sorted MG

We crossed *Tg(lws2: nfsb-mCherry)* with *Tg(pcna: GFP)*, *Tg(her4.1: dRFP)*, *Tg(gfap: EGFP)*, and *Tg(cxcl18b: GFP)* to collect retina cell. the retinas were dissected and the cells dissociated for sorting and enrichment of signal-positive cells using fluorescence-activated cell sorting (FACS, Beckman, MoFlo XDP). After 72 hours post G/R cone ablation, GFP^+/RFP^+ cells were collected from the retinas of *Tg(lws2: nfsb-mCherry* x *pcna: GFP)* as the proliferative MG group. For the uninjured MG group, GFP^+/RFP^+ cells were collected from *Tg(lws2: nfsb-mCherry* x *gfap: EGFP* x *her4.1: dRFP)* uninjured retinas, while GFP^+/RFP^+ cells from injured retinas represented the 72-hpi MG group, while GFP^-/RFP^- cells were enriched as the

other retinal cell types group in the 72 hpi retinas. Additionally, from *Tg(lws2: nfsb-mCherry* x *cxcl18b: GFP)* retinas, GFP^+/RFP^+ cells were collected as the *cxcl18b*$^+$ MG group and single RFP^+ cells as the G/R cone group at 72 hpi **(Figure 5A)**.

Interesting cells were collected into a 1.5-ml tube containing lysis buffer (20 mg/ml PK in TE buffer) and total RNA was isolated using this lysis buffer. cDNA synthesis was conducted by adding RT mix contains: 200 U Superscript II reverse transcriptase (Invitrogen, 18064-014), 1 × First-strand buffer (Invitrogen, 18064-014), 5 mM DTT (Invitrogen, 18064-014), 20 U Recombinant RNase inhibitor (Clontech, 2313A), 6 mM MgCl2 (Sigma, M8266), 1 μM TSO**(Picelli et al., 2013)**; 8% PEG8000 (Sigma, P1458). PCR amplification was performed as previously described**(Picelli et al., 2013)**.

Real-time quantitative PCR (RT-qPCR) reactions were carried out using TB Green Premix Ex Taq (Takara, RR420A) on a LightCycler 480 II real-time PCR detection system (Roche). The qPCR primers are listed in **Supplementary Table S3**. The ΔΔCt method was used to determine the relative expression of mRNAs in different group retinae cells and normalized to *actin* mRNA levels. Each group comparison was performed using a two-way ANOVA followed by Tukey's HSD test. Error bars represented SEM. ****$p<0.0001$, ***$p<0.001$; **$p<0.01$; *$p<0.05$; ns, $p>0.05$.

Construction and injection of adenoviral-based MG-specific knockout system in the zebrafish retina

The type of AdC68 used in our study is a replication-deficient chimpanzee adenovirus. The plasmids used for viral packaging were described above, and the amplification and purification of recombinant chimpanzee adenovirus followed the standard protocol**(Jia et al., 2019; Liu et al., 2021)**. We generated four adenoviruses for this study, including *AdC68XY2-E1-CMV-GFP pAdC68XY2-E1-10xUAS: Cas9-2a-Cre-U6: sgRNA1(nos2b)*; *U6: sgRNA2(nos2b)* (referred to as *UAS: Cas9-2a-Cre-sgnos2b*, infectious titer: 2.00 x 10^{13} ifu/ml)*, pAdC68XY2-E1-cxcl18b: gal4FF* (referred to as *cxcl18b: gal4*, infectious titer: 1.90 x 10^{13} ifu/ml) and *pAdC68XY2-E1-*

10xUAS: Cas9-2a-Cre-U6: empty (referred to as *UAS: Cas9-2a-Cre*, infectious titer: 1.75 x 10^{13} ifu/ml) as a control.

All adenoviruses were diluted in sterile PBS to a final infectious titer: 1.00 x 10^{13} ifu/ml. The *UAS: Cas9-2a-Cre-sgnos2b* and *cxcl18b: gal4* adenoviruses were mixed at a 1:1 ratio for the MG-specific knockout system, while the *UAS: Cas9-2a-Cre* with *cxcl18b: gal4* adenoviruses were similarly mixed as a control. To achieve the *cxcl18b*$^{+}$ MG cell-specific knockout *nos2b*, we performed the intravitreal injection of the adenovirus mixtures into the eyes of *Tg(ef1α: loxP-DsRed-loxP-EGFP* x *lws2: nfsb-mCherry)* at 5 dpf. One day post-injection, the fish were treated with MTZ for 3 consecutive days to ablate the G/R cone **(Figure 6E)**.

Tissue preparation and immunostaining

Zebrafish were fixed in 4% paraformaldehyde (PFA, Electron Microscopy Services, 157–8) overnight, then cryoprotected in 30% sucrose for 6 hours, flash-frozen, and cryosectioned at a thickness of 14 μm. Immunostaining was performed following the protocol described by Tang et al.**(Tang et al., 2017)**. The primary antibody including mouse anti-PCNA (Abcam, ab29) at a 1:500 dilution, as well as mouse anti-GS (glutamine synthase, BD Transduction Laboratories, 610518), rabbit anti-BLBP (Abcam, ab32423), rabbit anti-DsRed (Clontech, 632496), rabbit anti-TaqGFP (Proteintech, 50430-2-AP), and chicken anti-GFP (Abcam, ab13970) each at a 1:1000 dilution. Secondary antibodies conjugated to Alexa Fluor 488, 594, or 647 (Jackson ImmunoResearch Laboratories Inc.) were used at a 1:1000 dilution. Primary antibodies were incubated overnight at 4°C, while Alexa Fluor secondary antibodies were incubated at room temperature for 2 hours. DAPI staining was performed according to the standard protocol.

In situ hybridization

In this study, three digoxigenin (DIG)-labeled RNA probes targeting endogenous *cxcl18b, fabp11a,* and *col15α1b* were synthesized using the MEGAscript™ T7 High Yield Transcription Kit (Invitrogen, AM1334) and the DIG RNA Labeling Kit (Roche,

11277073910), following the manufacturer's instructions. The cDNA of each gene was amplified by PCR using the following primers: *cxcl18b* -F: 5'-ATGGCATTCACACCCAAAGCG-3'; *cxcl18b* -R: 5'-TAATACGACTCACTATAGGGATTGGCCCTGCTGTTTTTGTG-3'; *fabp11a*-F: 5'-GTTGGAAACCGGACCAAACC-3'; *fabp11a*-R: 5'-TAATACGACTCACTATAGGGACGGCTCGTTGAGCTTGAAT-3'; *col15a1b* -F: 5'-CCTCAATGGAGGTCCTAAAGGT-3'; *col15α1b* -R: 5'-TAATACGACTCACTATAGGGACCAGCTTCTGAGACCAAGC-3'.

Following the *in situ* hybridization protocol described by Tang et al.**(Tang et al., 2017)**, fresh zebrafish retinal sections were incubated overnight in the HybEZ system (Advanced Cell Diagnostics, 310013) at 65°C with 200 ng of probe for each slide. The next day, slides were sequentially washed in 5x SSC buffer and incubated overnight at 4°C with an anti-DIG-POD antibody (Roche, 11093274910) diluted 1:500 in TNB buffer (TN buffer with 0.5% blocking reagent; Roche). On the third day, the signal was detected using the TSA™ Plus Cyanine 3 (PerkinElmer, NEL744001KT) or Cyanine 5 (PerkinElmer, NEL745001KT)/Fluorescein System.

Imaging

Images were taken using an inverted confocal microscope system (FV1200, Olympus) confocal microscope using 40 × (silicon oil, 1.05 NA), or 60 × (silicon oil, 1.3 NA) objectives.

Quantifications and statistical analysis

All quantification and visualization were performed with FV31S-SW 2.3.1.163 Viewer (Olympus), and ImageJ. ***Z intensity projection*** was used to process the Z-stack images acquired from 14-μm-thick sections of zebrafish retina for statistical analysis. For cell counting, $PCNA^+$ MG and their lineage in this study were defined as one proliferative MG, *cxcl18b*$^+$ MG and their lineage were counted as one *cxcl18b*$^+$ MG.

To perform the statistical analysis, p values were calculated with GraphPad Prism 8 (or Microsoft Excel). The unpaired, non-parametric Wilcoxon test was applied for comparison of two groups. The one-way ANOVA, followed by Tukey's HSD test was applied for comparison of different groups with one treatment. The two-way ANOVA followed by Tukey's HSD test was applied for comparison of four groups with two treatments. Error bars represent SEM. ****$p<0.0001$, ***$p<0.001$; **$p<0.01$; *$p<0.05$; ns, $p>0.05$.

882 # Main Figure Titles and Legends

883 **Figure 1. Single-cell RNA seq reveals injury-induced the *cxcl18b*-defined MG**
884 **transitional states**

885 **(A)** Schematic showing the experimental procedure: five consecutive days of MTZ
886 treatment in *Tg(lws2: nfsb-mCherry* x *mpeg1: GFP)* fish to ablate green and red
887 (G/R) cone, starting at 6 dpf and continuing until 11 dpf. The MTZ solution was
888 refreshed every 24 hours, followed by fish fixation for further immunostaining.
889 **(B-D)** Quantitative plots showing the dynamic changes in the number of G/R cone
890 **(B)**, recruited microglia **(C)**, and proliferative MG ($PCNA^+$) **(D)** at different time
891 points after MTZ treatment (uninjured: collected retina number n=14; 24-hpi: n=10;
892 48-hpi: n=10; 72-hpi: n=11; 96-hpi: n=12; 120-hpi: n=16; mean ± SEM;
893 ****p<0.0001, ***p<0.001, **p<0.01, ns, p>0.05; one-way ANOVA followed by
894 Tukey's HSD test).
895 **(E)** Representative images showing microglia recruitment (*mpeg1: GFP*, green), G/R
896 cone ablation (*lws2: nfsb-mCherry*, red), and injury-induced MG proliferation
897 (PCNA, white) in uninjured **(E_1)** and 72-hpi **(E_2)** retinas. The high-magnification
898 images of the boxed area **(E_3-E_4)**. Scale Bars: 20 μm **(E_1, E_2)**, 10 μm **(E_3)**, 2 μm **(E_4)**.
899 **(F)** The UMAP plot of 4,172 MG cells was sorted with an increased proportion in
900 response to the G/R cone ablation. Cells were further aggregated into 10 clusters
901 based on previously published scRNA-seq data**(Krylov et al., 2023)**.
902 **(G)** Pseudo-time developmental trajectory of MG states identified by Monocle2
903 analysis shows a main developmental branch originating from Cluster 4 (*cx43*$^+$),
904 which diverges into two sub-branches: Cluster 0 and Clusters 5/3/6 (*pcna*$^+$).
905 **(H)** Violin plots showing the expression levels of key genes (*cx43*, *glula*, *gfap*,
906 *cxcl18b*, *ascl1α*, *mki67*, *pcna*, and *notch3*) in the main developmental branch clusters,
907 progressing from the most original MG states (Cluster 4) to transitional MG states
908 (Clusters 1/2/5), and proliferative MG states (Clusters 3/6).
909

910 **Figure 2. Clonal analysis reveals the proliferative MG mostly originated from**
911 ***cxcl18b*$^+$ MG transitional states**

912 **(A)** Representative images show dynamic expression of *cxcl18b* (red, *in situ*
913 hybridization) and PCNA (white, immunostaining) in *Tg(lws2: nfsb-mCherry)* retina
914 at different time points following the G/R cone ablation. Scale bars: 20 μm.
915 **(B)** Quantitative plots showing the number of *cxcl18b*$^+$ (red curve, significance shown
916 above the curve) and $PCNA^+$ MG (blue curve, significance shown below the curve) in
917 uninjured (n=11) and injured retina at 24-hpi (n=10), 48-hpi (n=12), 72-hpi (n=11),
918 96-hpi (n=7), and 120-hpi (n=5). Each injured time point was compared to the
919 uninjured retina (Mean ± SEM; ****p<0.0001, **p<0.01, ns, p>0.05; one-way
920 ANOVA followed by Tukey's HSD test).

921 **(C)** Schematic diagram of the *cxcl18b* promoter was used to construct the reporter
922 fish line *Tg(cxcl18b: GFP)* and clonal analysis fish line *Tg(cxcl18b: Cre-vmhc-*
923 *mCherry:: ef1α: loxP-DsRed-loxP-EGFP; lws2: nfsb-mCherry)*.
924 **(D)** Immunostaining of injury-induced *cxcl18b*$^+$ (green, indicated by *Tg(cxcl18b:*
925 *GFP)*) and proliferative (PCNA$^+$, white) MG showing overlapping in the central
926 retina area (yellow arrows, GFP$^+$/PCNA$^+$ MG) at 48 hpi. The high-magnification
927 images of the boxed area **($D_{3'}$-$D_{3'''}$)**. The area of the retina is labeled with a dashed
928 line, and each layer structure is labeled with dashed lines and marked with the outer
929 nuclear layer (ONL), inner nuclear layer (INL), inner plexiform layer (IPL), ganglion
930 cell layer (GCL) and lens. Scale Bars: 20 μm **(D_1-D_2)** and 5 μm **($D_{3'}$-$D_{3'''}$)**.
931 **(E)** Quantitative plots showing the number of *cxcl18b*$^+$ MG (red) and proliferative
932 MG (PCNA$^+$, blue) in **(D_1)** uninjured (n=4) and **(D_2)** 48-hpi retina (n=7) (Mean ±
933 SEM; ****p<0.0001, ns, p>0.05; two-way ANOVA followed by Tukey's HSD test).
934 **(F)** Clonal analysis of injury-induced *cxcl18b*$^+$ MG in transgenic fish line *Tg(cxcl18b:*
935 *Cre-vmhc: mCherry:: ef1α: loxP-DsRed-loxP-EGFP:: lws2: nfsb-mCherry)* at 72 hpi
936 retina showing overlapping between proliferative (PCNA$^+$, white) MG with *cxcl18b*$^+$
937 (green, yellow arrows). The high-magnification images of the boxed area **($F_{3'}$-$F_{3'''}$)**.
938 Scale Bars: 20 μm **(F_1-F_2)** and 5 μm **($F_{3'}$-$F_{3'''}$)**.
939 **(G)** Quantitative analysis at 72 hpi shows no significance in the number of
940 proliferative MG (PCNA+, blue) and double-positive (PCNA$^+$ / *cxcl18b*$^+$, red) MG
941 (n=14; Mean ± SEM; ns, p>0.05; Unpaired t-test) in **(F)**, with 93±2% of PCNA$^+$ MG
942 also being *cxcl18b*$^+$.
943 **(H)** Representative images show that not all mature MG stained with glutamate
944 synthase (GS$^+$, magenta) are *cxcl18b*$^+$ (green, labeled by *cxcl18b*: Cre) in the central
945 retinal area (white dashed lines identified a 45° angular region originating from the
946 optic nerve). The high-magnification images of the boxed area **($H_{2'}$-$H_{2'''}$)**. Scale Bars:
947 20 μm **(H_1)** and 5 μm **($H_{2'}$-$H_{2'''}$)**.
948 **(I)** Quantification of GS$^+$/*cxcl18b*: Cre$^+$ double-positive (blue, yellow arrows in **H**)
949 and GS$^+$/*cxcl18b*: Cre$^-$ single-positive (red, open yellow arrowheads in **H**) MG (n=14,
950 Mean ± SEM; *p<0.05; one-way ANOVA followed by Tukey's HSD test), and the
951 proportion of *cxcl18b*: Cre$^{+\text{ or }-}$ MG within the total population of mature (GS$^+$) MG in
952 the central retina.
953 **(J_1-J_3)** Representative images showing injury-induced *cxcl18b*$^+$ MG (green) in
954 *Tg(lws2: nfsb-mCherry x cxcl18b: GFP)* fish retina treated with dexamethasone (Dex)
955 or DMSO at 72 hpi. Scale bars: 20 μm.
956 **(K-M)** Quantitative plots showing the number of *cxcl18b*$^+$ MG (72 hpi: n=14; DMSO:
957 n=6, Dex: n=10) in **J_1-J_3**; recruited microglia in **Figure 2-figure supplement 1J_1-J_3**
958 and proliferative MG in **Figure 2-figure supplement 1J_4-J_6** (72 hpi: n=9; DMSO:
959 n=7, Dex: n=14) in *Tg(mpeg1: GFP; lws2: nfsb-mCherry)* retinas after DMSO or Dex
960 treatment at 72 hpi (Mean ± SEM; ****p<0.0001, ***p<0.001, ns, p>0.05; one-way
961 ANOVA followed by Tukey's HSD test).
962

963 **Figure 3. The *cxcl18b*-defined MG transitional states recapitulate the**

964 **developmental states of RSCs in the CMZ**

965 **(A, C)** UMAP plots display 5,368 retinal progenitor cells (RPCs) at 24 hpf and 4,625
966 CMZ progenitor cells at 14 dpf. Clusters are indicated by their cluster-specific marker
967 genes based on previously published scRNA-seq data**(Xu et al., 2020)**.
968 **(B, D)** UMAP plots showing expression of *fabp11a*, *cxcl18b*, and *col15α1b* at r24-hpf
969 RPCs (embryonic states) **(B)** and r14-dpf CMZ-progenitors (post-embryonic states)
970 **(D)**.
971 **(E-H_3)** *In situ* hybridization images showing the expression of *fabp11a* (green),
972 *col15α1b* (white), two putative makers for post-embryonic retinal stem cells (RSCs),
973 and *cxcl18b* at 30-hpf **(E-F_3)** and 14-dpf **(G-H_3)** retina. The high-magnification
974 images of the boxed area **(F-F_3, H-H_3)**. The area of these three in situ signal trouble
975 positive is labeled with a dashed yellow line. Scale Bars: 20 μm **(E, G)** and 3 μm **(F-**
976 **F_3, H-H_3)**.
977

978 **Figure 4. The nitric oxide metabolic pathway regulates injury-induced MG**

979 **proliferation**

980 **(A)** Representative images of microglia recruitment (green, marked by *Tg(mpeg1:*
981 *GFP)*), G/R cone ablation (red, marked by *Tg(lws2: nfsb-mCherry)*) and proliferative
982 MG (white, marked by $PCNA^+$) at 72 hpi with nitric oxide metabolism pathway genes
983 disruption (*nos1*/*nos2a*/*nos2b*/*gsnor*). Scale Bars: 20 μm.
984 **(B)** Quantitative analysis of the number of proliferative MG ($PCNA^+$) at 72 hpi in
985 **(A)**. In total, we collected 11 retinas for WT (n=11), *scramble* sgRNA-injection (n=7),
986 *nos1* sgRNA-injection (n=23), *nos2a* sgRNA-injection (n=15), *nos2b* sgRNA-
987 injection (n=22), and *gsnor* sgRNA-injection (n=13) (Mean ± SEM; ****$p<0.0001$,
988 **$p<0.01$, *$p<0.05$, ns, $p>0.05$; one-way ANOVA followed by Tukey's HSD test).
989 **(C)** Schematic showing the experimental procedure of nitric oxide synthase (*Nos*)
990 inhibitors injection or NO scavengers treatment in *Tg(lws2: nfsb-mCherry* x *mpeg1:*
991 *GFP)* retina starting from 5 dpf for five consecutive days to 10 dpf with three
992 consecutive days of MTZ treatment for G/R cone ablation from 7 dpf to 10 dpf. *Nos*
993 inhibitors, NO scavengers, and MTZ solution were refreshed every 24 hours, and fish
994 fixation was at 10 dpf for further immunostaining.
995 **(D)** Representative images of microglial recruitment (green, marked by *Tg(mpeg1:*
996 *GFP)*), G/R cone ablation (red, marked by *Tg(lws2: nfsb-mCherry)*) and proliferative
997 MG (white, marked by $PCNA^+$) at 72 hpi following L-NMMA (10 mM), L-NAME
998 (10 mM), 1400W (200 nM) intravitreal injection, and PBS as control, or C-PTIO (10
999 mM) treatment. Scale Bars: 20 μm.
1000 **(E)** Quantitative plots showing the number of proliferative ($PCNA^+$) MG at 72 hpi in
1001 **(D)**. Retinas analyzed WT (n=11), PBS-injected (n=16), L_NMMA-injected (n=12),
1002 L_NAME-injected (n=12), 1400W-injected (n=10), and C-PTIO treatment (n=27)
1003 (Mean ± SEM; ****$p<0.0001$, ns, $p>0.05$; one-way ANOVA followed by Tukey's
1004 HSD test).

1005 **(F-G)** Representative images of proliferative MG (PCNA$^+$, white) and G/R cone
1006 ablation (marked by *Tg(lws2: nfsb-mCherry)*, red) at 72 hpi in heterozygous (*nos1*$^{+/-}$,
1007 *nos2a*$^{+/-}$, *nos2b*$^{+/-}$, *gsnor*$^{+/-}$) **(F)** and homozygous mutants **(G)** of nitric oxide
1008 metabolism pathway genes (*nos1*$^{-/-}$, *nos2a*$^{-/-}$, *nos2b*$^{-/-}$, *gsnor*$^{-/-}$). Scale Bars: 20 μm.
1009 **(H-I)** Quantitative plots showing the number of proliferative MG (white, PCNA$^+$) at
1010 72 hpi in *nos* and *gsnor* mutant fish. In heterozygous **(H)**, analyzed retinas include
1011 WT (n=14), *nos1*$^{+/-}$ (n=19), *nos2a*$^{+/-}$ (n=13), *nos2b*$^{+/-}$ (n=20), *gsnor*$^{+/-}$ (n=12). For
1012 homozygous **(I)**, analyzed retinas include *nos1*$^{-/-}$ (n=18), *nos2a*$^{-/-}$ (n=20), *nos2b*$^{-/-}$
1013 (n=20), *gsnor*$^{-/-}$ (n=27) (Mean ± SEM; ****p<0.0001, ns, p>0.05; one-way ANOVA
1014 followed by Tukey's HSD test).
1015 **(J-K)** Quantitative plots showing the number of proliferative MG (white, PCNA$^+$) **(J)**
1016 and photoreceptor cells remain **(K)** at 72 hpi in *nos2b* hetero- or homozygous
1017 mutants. (Mean ± SEM; ****p<0.0001, ***p<0.001, ns, p>0.05; one-way ANOVA
1018 followed by Tukey's HSD test).
1019

1020 **Figure 5. RT-qPCR analysis reveals *nos2b* cell-specific expression in the injury-**

1021 **induced *cxcl18b*$^+$ MG**

1022 **(A)** Schematic showing the workflow for isolating and enriching for three post-injury
1023 MG populations (72-hpi MG, 72-hpi PCNA$^+$ MG, and 72-hpi *cxcl18b*$^+$ MG) and three
1024 control groups (uninjured MG, 72-hpi retinal cells other than MG, and 72-hpi G/R
1025 cones) using fluorescence-activated cell sorting (FACS).
1026 **(B-C)** RT-qPCR analysis of *nos1*, *nos2a*, *nos2b*, and *gsnor* expression in different cell
1027 populations. Expression levels are shown relative to 72-hpi G/R cones **(B)** and other
1028 72-hpi retinal cell types **(C)**. A total of six independent replicates were performed for
1029 cell population enrichment and cDNA template preparation (n=6, Mean ± SEM;
1030 ****p<0.0001, ns, p>0.05; two-way ANOVA followed by Tukey's HSD test).
1031 **(D)** RT-qPCR analysis comparing *nos1*, *nos2a*, *nos2b*, and *gsnor* expression in
1032 distinct MG states relative to uninjured MG (repeats n=7 in *cxcl18b*$^+$ MG; n=5 in 72-
1033 hpi MG; and repeats n=6 in PCNA$^+$ MG; n=6 in the uninjured retina; Mean ± SEM;
1034 ****p<0.0001, ns, p>0.05; two-way ANOVA followed by Tukey's HSD test).
1035

1036 **Figure 6. NO produced by *nos2b* in *cxcl18b*$^+$ MG regulates injury-induced**

1037 **proliferation**

1038 **(A-C)** Representative images showing the adenovirus-mediated infection (green,
1039 indicated by Y_2-GFP) specifically target MG (red, GS staining) in the zebrafish retina.
1040 The virus was intravitreally injected into the right eye of *Tg(lws2: nfsb-mCherry* x
1041 *ef1α: loxP-DsRed-loxP-EGFP)* fish **(A_2, C)**, with the left eye as a wild-type (WT)
1042 control **(A_1)**. The high-magnification images of the boxed area (B-B_3). Scale Bars:
1043 20 μm (A_1, A_2) and 5 μm (B-B_3).
1044 **(D)** Schematic showing the design of the *cxcl18b*$^+$ MG-specific *nos2b* knockout

system. The viral construct consists of three plasmids: (1) *gal4* expression driven by the *cxcl18b* promoter; (2) *UAS*-derived *Cas9* and *Cre* elements, and (3) *U6* promoters driving two sgRNAs targeting *nos2b*, with a non-targeting sgRNA as the control.
(E) Schematic showing the procedure of injury process and intravitreal viral injection in *Tg(lws2: nfsb-mCherry* x *ef1α: loxP-DsRed-loxP-EGFP)* fish.
(F-G) Representative images showing proliferative MG ($PCNA^+$, white) with *cxcl18b*$^+$ MG specific knockout *nos2b* in **(G)** and control in **(F)**, (GFP^+, green, yellow arrows) are defined as virus-infected clones. Upper panels show WT retina (no virus injected),
Bottom panels show retinas injected with the virus (two sgRNA targets as *nos2b* knockout and without sgRNA targets as control). Scale Bars: 20 μm.
(H) Quantification of proliferative ($PCNA^+/GFP^+$, red bars) and non-proliferative ($PCNA^-/GFP^+$, gray bars) MG clones in (**F**). For control, ~75% of virus-infected clones entered the cell cycle ($PCNA^+$; red bars), with 90/120 clones analyzed across 8 independent experiments (n=8). For *nos2b* knockout clones, ~23% entered the cell cycle ($PCNA^+$; blue bars), with 22/103 clones analyzed across 6 independent experiments (n=6) (Mean ± SEM; ****p<0.0001; two-way ANOVA followed by Tukey's HSD test).

Figure 7. NO regulates MG proliferation by suppressing Notch signaling

(A) Dot plot showing the Notch signaling-related gene expression in different MG states. The average expression levels of these genes for all cells in each cluster are coded by the gray level. The percentage of cells expressing each gene within each cluster is coded by dot size.
(B) Representative images showing the dynamic changes of Notch signaling activity (green, indicated by *Tg(Tp1: EGFP)*) and proliferative MG (white, $PCNA^+$) following injury with nitric oxide (NO) blockade using C-PTIO. Scale Bars: 20 μm.
(C-D) Quantitative plots showing the number of Notch activation (*tp1*: GFP^+ MG) in **(C)** and proliferative MG ($PCNA^+$ MG) in **(D)** at different time points post-G/R cone ablation. We collected uninjured retina (24-hpi, n=4; 48-hpi, n=4; 72-hpi, n=3), injured retina (24-hpi, n=9; 48-hpi, n=4; 72-hpi, n=6), and retina treated with C-PTIO (24-hpi, n=6; 48-hpi, n=5; 72-hpi, n=7) (Mean ± SEM; ****p<0.0001, ***p<0.001, **p<0.01, *p<0.05, ns, p>0.05; two-way ANOVA followed by Tukey's HSD test).

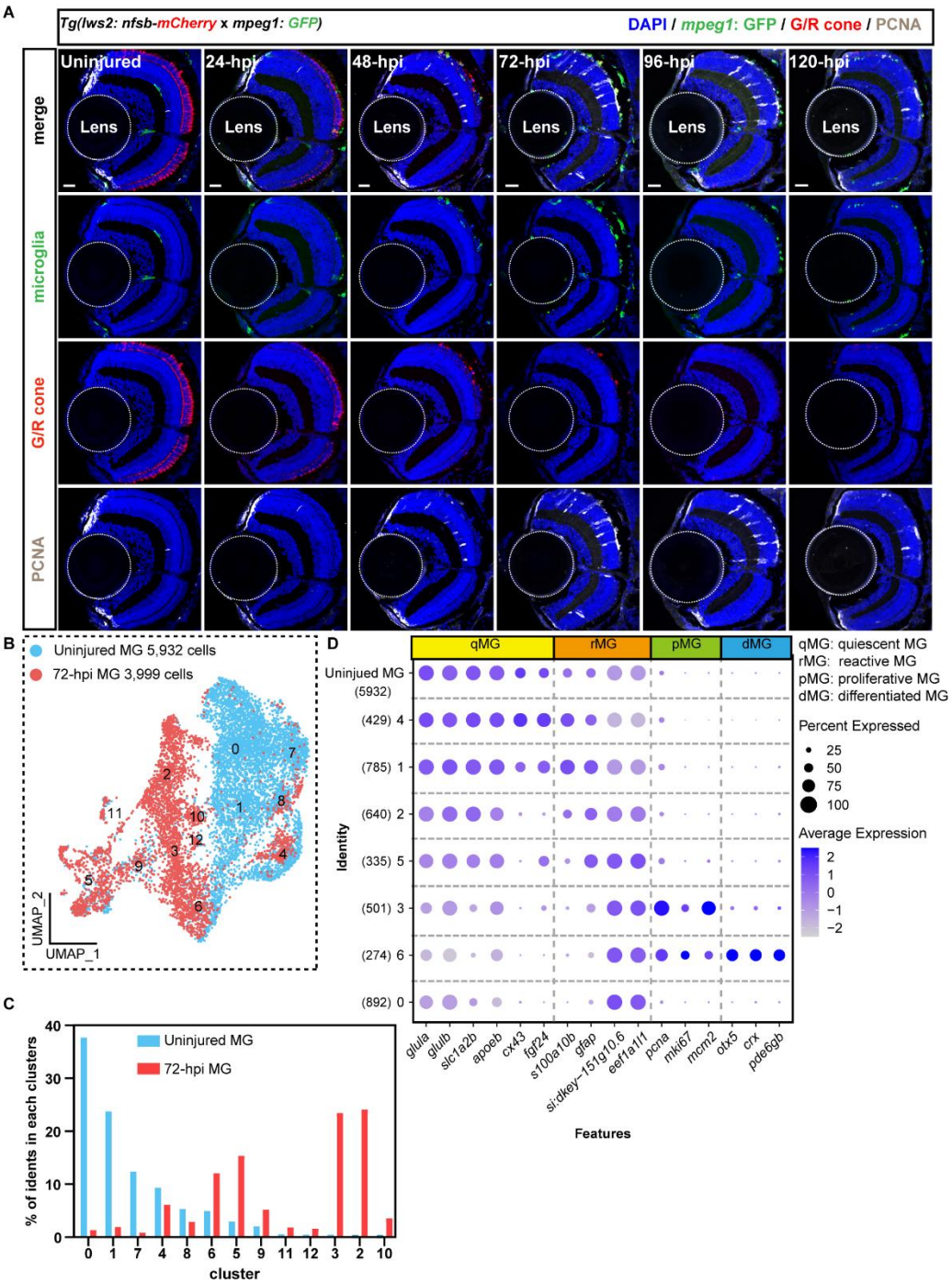

Figure 1-figure supplement 1. Clusters with increased proportion are identified from the scRNA-seq data

(A) Representative images showing microglia recruitment (green, indicated by *Tg(mepg1: GFP)*), G/R cone ablation (red, *Tg(lws2: nfsb-mCherry)*), and injury-induced MG proliferation (white, marked by PCNA) following the injury process from uninjured retina to 120 hpi. Scale Bars: 20 μm.

(B) UMAP plot showing 5,932 cells from uninjured retinas (blue) and 3,999 cells from 72-hpi (red) retinas were obtained, which further aggregated into 13 clusters.

1088 **(C)** Percentage of MGs from uninjured and 72-hpi retinas in each cluster. Eight
1089 clusters (6, 5, 9, 11, 12, 3, 2, 10) were identified and showed an increased proportion
1090 for further analysis.
1091 **(D)** Dot plot showing the expression levels of marker genes for quiescent MG (qMG),
1092 reactive MG (rMG), proliferative MG (pMG), and differentiated MG (dMG). The
1093 average expression levels of these genes for all cells in each cluster are coded by the
1094 gray level. The percentage of cells expressing each gene within each cluster is coded
1095 by dot size.
1096

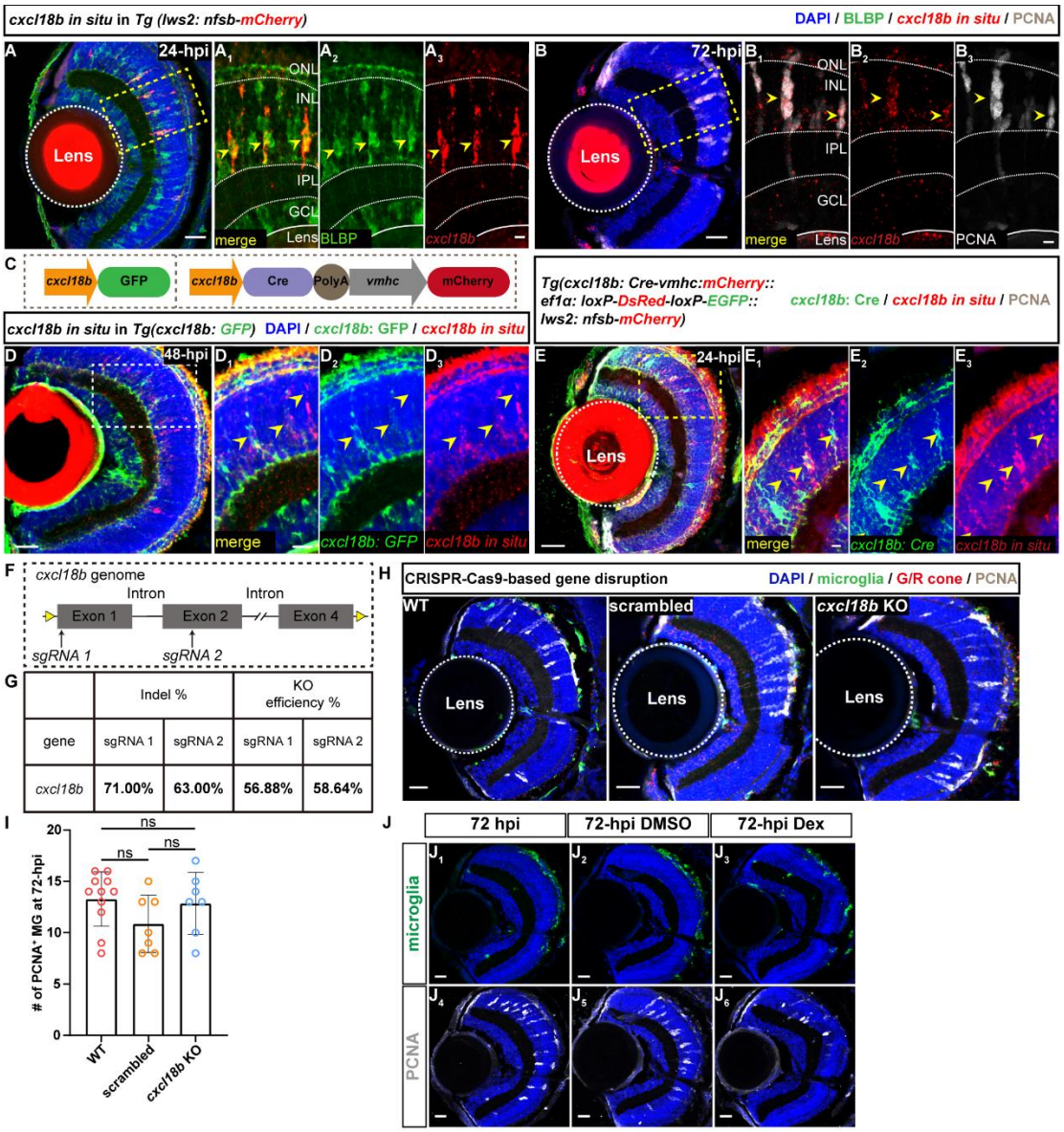

Figure 2-figure supplement 1. Gene description of *cxcl18b* does not reduce MG proliferation

(A-A$_3$) *In situ* hybridization images show injury-induced *cxcl18b* (red, marked by *in situ* hybridization) with MG-like morphology, cell-specific expressed in the BLBP$^+$ cells (green, labeled by immunostaining) at 24 hpi in the transgenic fish line *Tg(lws2: nfsb-mCherry)* retina. In these clones, *cxcl18b*$^+$ MG are red$^+$/BLBP$^+$ cells (yellow arrowheads). The high-magnification images of the boxed area **(A$_1$-A$_3$)**. The area of the retina structure is labeled with a dashed line, and each layer structure is labeled with dashed lines and marked with the outer nuclear layer (ONL), inner nuclear layer (INL), inner plexiform layer (IPL), ganglion cell layer (GCL) and lens. Scale Bars: 20 μm **(A)** and 5 μm **(A$_1$-A$_3$)**.

(B-B$_3$) Representative images showing *cxcl18b* (red, *in situ* hybridization) co-expressed with PCNA (white, immunostaining) at 72 hpi. In these clones, *cxcl18b*$^+$

MG was identified as red$^+$/PCNA$^+$ cells (yellow arrowheads). The high-magnification images of the boxed area **(B_1-B_3)**. Scale Bars: 20 μm **(B)** and 5 μm **(B_1-B_3)**.

(C) Schematic showing the design of *cxcl18b* report fish line and the Cre-loxP transgenic fish line used for clone analysis. The *cxcl18b* promoter drives GFP or Cre expression, with the heart labeled by mCherry under the *vmhc* promoter for fish screening.

(D-E_3) Representative images showing *cxcl18b* expression labeled by *Tg(cxcl18b: GFP)* (green) in **(D-D_3)** at 48 hpi, or three transgenic fish *Tg(cxcl18b: Cre-vmhc: mCherry:: ef1α: loxP-DsRed-loxP-EGFP:: lws2: nfsb-mCherry)* (green) in **(E-E_3)** at 24 hpi fish retina, merged with *cxcl18b* in situ hybridization signal (red) **(D-E_3)**. The high-magnification images of the boxed area **(D_1-D_3, E_1-E_3)**. Scale Bars: 20 μm **(D, E)** and 5 μm **(D_1-D_3, E_1-E_3)**.

(F) Schematic showing the two sgRNA target sites of the *cxcl18b* genome.

(G) Summary table showing the indel and knockout efficiency of the two sgRNAs targeting *cxcl18b*.

(H) Representative images of proliferative MG (PCNA$^+$, white) at 72 hpi in *Tg(lws2: nfsb-mCherry)* fish retina with *cxcl18b* disruption. Scale Bars: 20 μm.

(I) Quantitative plots showing the number of proliferative MG (PCNA$^+$) at 72 hpi in **H**. In total, retinas were collected from wild-type (WT, n=11), *scramble* sgRNA-injected (*scrambled*, n=7), and *cxcl18b* sgRNA-injected (*cxcl18b* KO, n=7) (Mean ± SEM; ns, $p>0.05$; one-way ANOVA followed by Tukey's HSD test).

(J_1-J_6) Representative images showing injury-induced microglia recruitment (green, marked by *Tg(mpeg1: GFP)*) **(J_1-J_3)**, and proliferative MG (white, marked by PCNA) **(J_4-J_6)** after dexamethasone (Dex) or DMSO treatment in the in *Tg(mpeg1: GFP x lws2: nfsb-mCherry)* fish retina at 72 hpi. Scale bars: 20 μm.

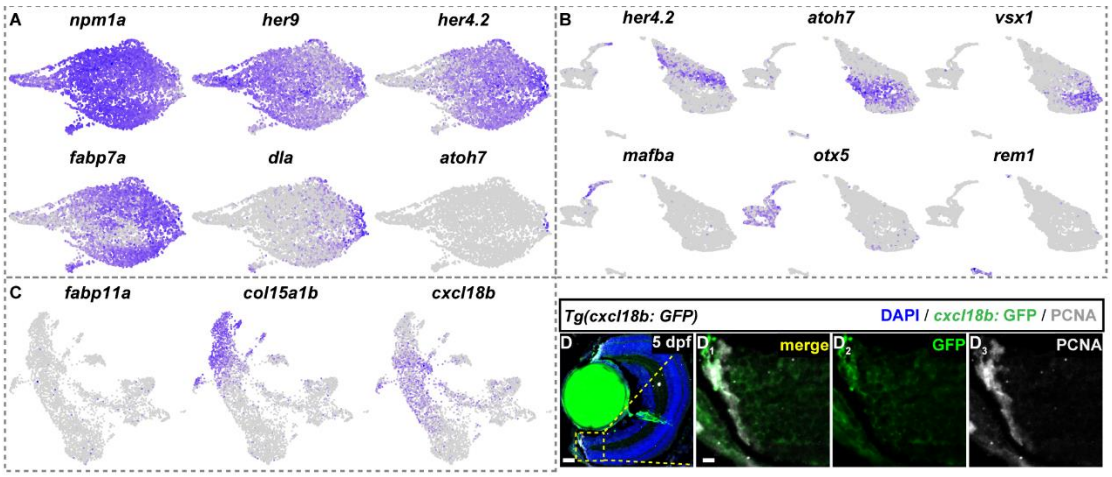

Figure 3-figure supplement 1. UMAP plots show the expression of cluster-specific marker genes utilized to identify developmental states

(A, B) UMAP plots showing the expression pattern of embryonic developmental stage cluster-specific marker genes (*npm1a*, *her9*, *her4.2*, *fabp7a*, *dla*, and *atoh7*) in **(A)** and post-embryonic developmental stage marker genes (*her4.2*, *atoh7*, *vsx1*, *mafba*, *otx5*, and *rem1*) in **(B)**.
(C) UMAP plots showing the expression pattern of *fabp11a*, *cxcl18b*, and *col15α1b* at MG clusters with increased population after G/R cone ablation at 72 hpi in Figure 1F.
(D) Representative images showing the *cxcl18b* expression (green, marked by *Tg(cxcl18b: GFP)*) are located in the most peripheral region of the CMZ (white, marked by PCNA) at 5 dpf. The high-magnification images of the boxed area **(D_1-D_3)**. Scale Bars: 20 μm **(D)** and 5 μm **(D_1-D_3)**.

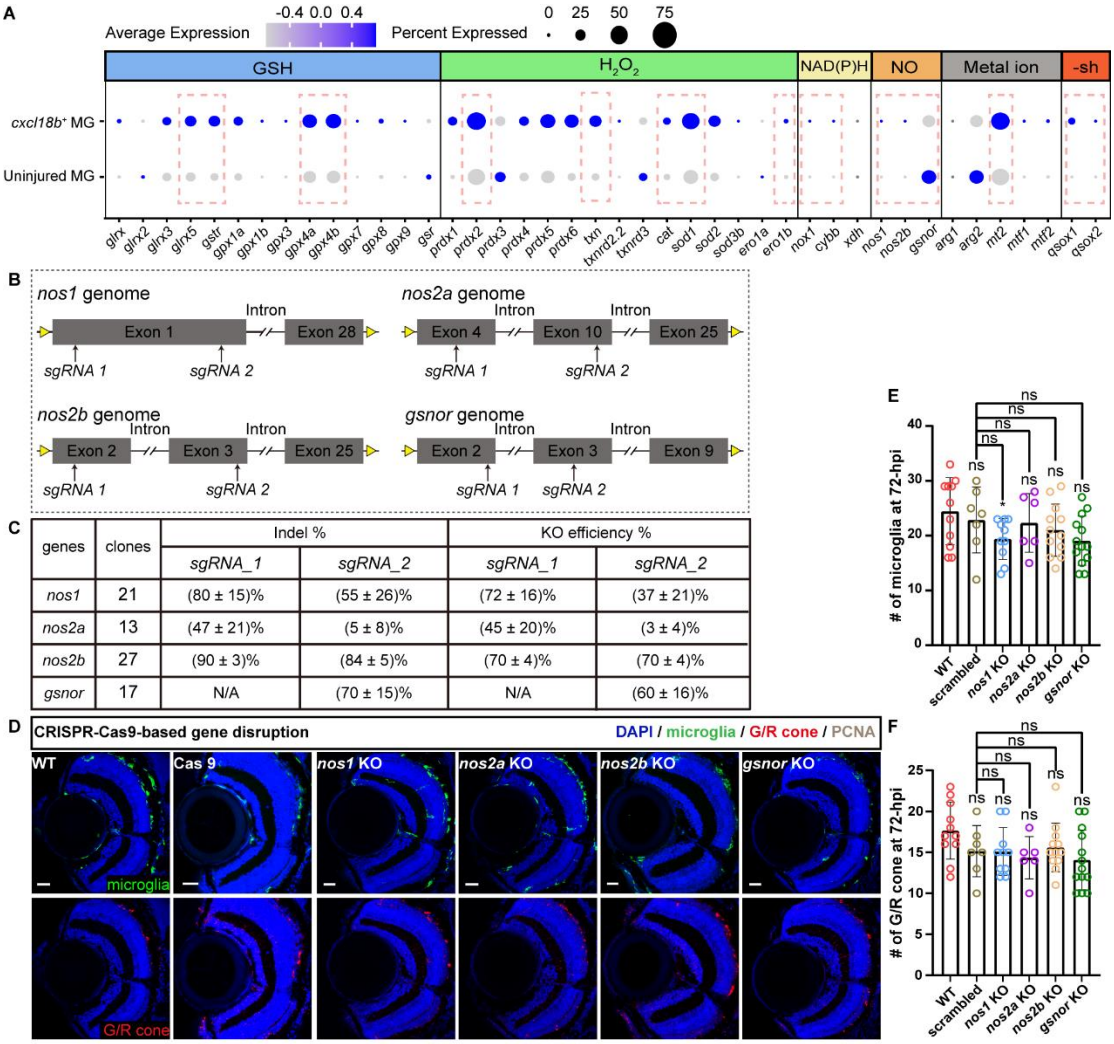

genes	clones	Indel %		KO efficiency %	
		sgRNA_1	*sgRNA_2*	*sgRNA_1*	*sgRNA_2*
nos1	21	(80 ± 15)%	(55 ± 26)%	(72 ± 16)%	(37 ± 21)%
nos2a	13	(47 ± 21)%	(5 ± 8)%	(45 ± 20)%	(3 ± 4)%
nos2b	27	(90 ± 3)%	(84 ± 5)%	(70 ± 4)%	(70 ± 4)%
gsnor	17	N/A	(70 ± 15)%	N/A	(60 ± 16)%

Figure 4-figure supplement 1. Genetic disruption of the nitric oxide pathway modulates G/R cone ablation and microglial recruitment

(A) Dot plot showing the redox gene expression profiles of regulating glutathione (GSH), hydrogen peroxide (H_2O_2), nicotinamide adenine dinucleotide phosphate (NADPH), nitric oxide (NO), metal ion, and sulfhydryl group (-SH) in the uninjured and *cxcl18b*$^+$ MG in 72-hpi scRNA-seq data **(Krylov et al., 2023)**. The average expression levels of these genes for all cells in each cluster were coded by the gray level. The percentage of cells expressing each gene within each cluster was coded by dot size.

(B) Schematic showing the two sgRNA target sites of the nitric oxide metabolism pathway genome (*nos1*/*nos2a*/*nos2b*/*gsnor*).

(C) Summary table showing the indel and knockout efficiency of the two sgRNAs targeting *nos1*/*nos2a*/*nos2b*/*gsnor*.

(D) Representative images of microglial recruitment (marked by *Tg(mpeg1: GFP)*, green) and G/R cone ablation (marked by *Tg(lws2: nfsb-mCherry)*, red) at 72 hpi with *nos1*/*nos2a*/*nos2b*/*gsnor* disruption, with *scrambled* sgRNA-injected as the control.

1169 Scale Bars: 20 μm.
1170 **(E-F)**. Quantitative plots showing the number of recruited microglia (GFP^+) **(D)** and
1171 G/R cone ablation ($mCherry^+$) **(E)** at 72 hpi with *nos1*/*nos2a*/*nos2b*/*gsnor* disruption.
1172 In total, we collected 11 retinas for WT (n=11), *scrambled* sgRNA-injected (n=7),
1173 *nos1* sgRNA-injected (n=10), *nos2a* sgRNA-injected (n=6), *nos2b* sgRNA-injected
1174 (n=12), and *gsnor* sgRNA-injected (n=13) (Mean ± SEM; *$p<0.05$; ns, $p>0.05$; one-
1175 way ANOVA followed by Tukey's HSD test).
1176

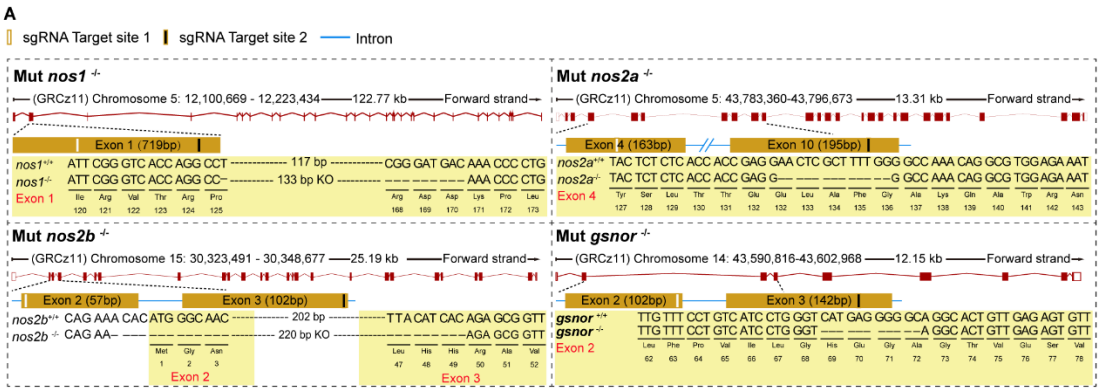
A
sgRNA Target site 1
sgRNA Target site 2
Intron
Mut nos1 -/-
(GRCz11) Chromosome 5: 12,100,669 - 12,223,434
122.77 kb
Forward strand
Exon 1 (719bp)
nos1+/+ ATT CGG GTC ACC AGG CCT ---------- 117 bp ---------- CGG GAT GAC AAA CCC CTG
nos1-/- ATT CGG GTC ACC AGG CC– ---------- 133 bp KO ---------- – – – – – – AAA CCC CTG
Exon 1
Ile Arg Val Thr Arg Pro
120 121 122 123 124 125
Arg Asp Asp Lys Pro Leu
168 169 170 171 172 173
Mut nos2a -/-
(GRCz11) Chromosome 5: 43,783,360-43,796,673
13.31 kb
Forward strand
Exon 4 (163bp)
Exon 10 (195bp)
nos2a+/+ TAC TCT CTC ACC ACC GAG GAA CTC GCT TTT GGG GCC AAA CAG GCG TGG AGA AAT
nos2a-/- TAC TCT CTC ACC ACC GAG G– – – – – – – – – – – G GCC AAA CAG GCG TGG AGA AAT
Exon 4
Tyr Ser Leu Thr Thr Glu Glu Leu Ala Phe Gly Ala Lys Gln Ala Trp Arg Asn
127 128 129 130 131 132 132 133 134 135 136 137 138 139 140 141 142 143
Mut nos2b -/-
(GRCz11) Chromosome 15: 30,323,491 - 30,348,677
25.19 kb
Forward strand
Exon 2 (57bp)
Exon 3 (102bp)
nos2b+/+ CAG AAA CAC ATG GGC AAC ---------- 202 bp ---------- TTA CAT CAC AGA GCG GTT
nos2b-/- CAG AA– – – – – – – – – – –

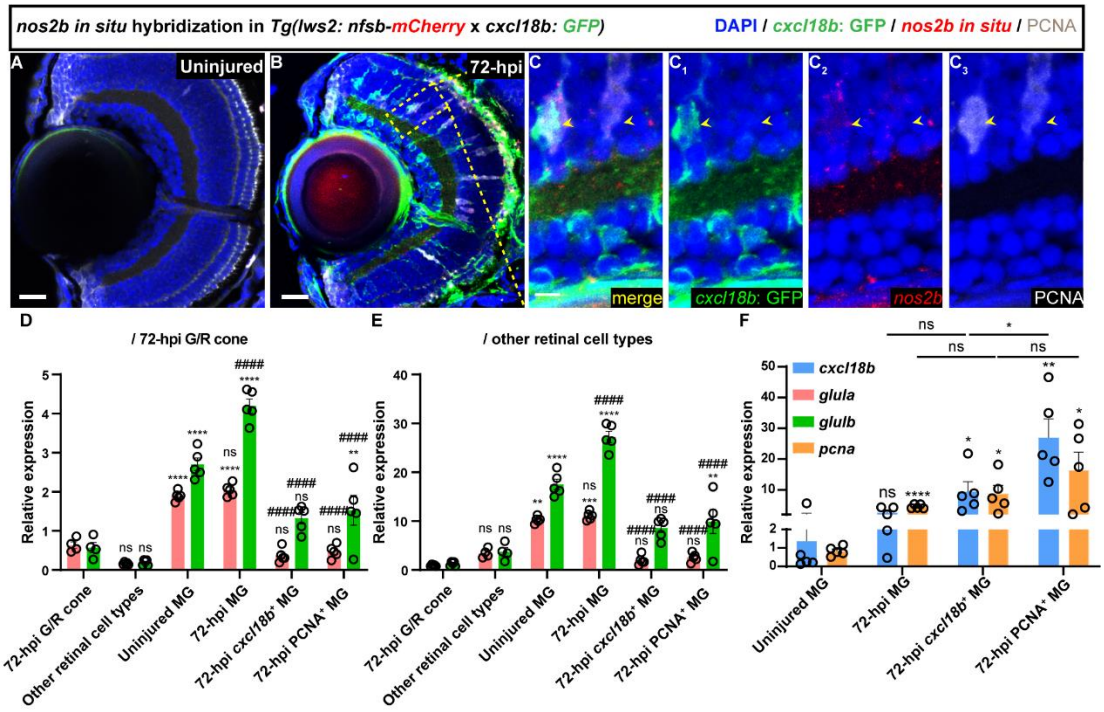

Figure 5-figure supplement 1. *In situ* hybridization reveals *nos2b* cell-specific expression in the *cxcl18b*-defined transitional MG states

(A-A$_3$) Representative *in situ* hybridization images showing *nos2b* expression (red, *in situ* hybridization) cell-specific in the injury-induced *cxcl18b*$^+$ MG (GFP$^+$, green) in *Tg(lws2: nfsb-mCherry* x *cxcl18b: GFP)* fish retina at 72 hpi. Clones with green/red/white trouble-positive are *cxcl18b*$^+$/*nos2b*$^+$/PCNA$^+$ MG cells (yellow arrowheads). The high-magnification images of the boxed area **(C-C$_3$)**. Scale Bars: 20 µm (A, B) and 5 µm **(C$_1$-C$_3$)**.

(D-E) RT-qPCR analysis of *glula* (pink bar) and *glulb* (green bar) expression in different cell populations relative to 72-hpi G/R cone **(D)**, or other retinal cell types **(E)**. The significance of 72-hpi G/R cone as control is noted by * for comparisons with 72-hpi G/R cones and # for comparisons with uninjured MG. In total, we do 6 independent replicates to enrich the different cell populations and get the cDNA templates (Mean ± SEM; **** and ####p<0.0001, **p<0.001, **p<0.01, ns, p>0.05; two-way ANOVA followed by Tukey's HSD test).

(F) RT-qPCR analysis of *cxcl18b* (blue bar) and *pcna* (orange bar) expression in different MG states. (Mean ± SEM; ****p<0.0001, **p<0.01, *p< 0.05, ns, p>0.05; two-way ANOVA followed by Tukey's HSD test).

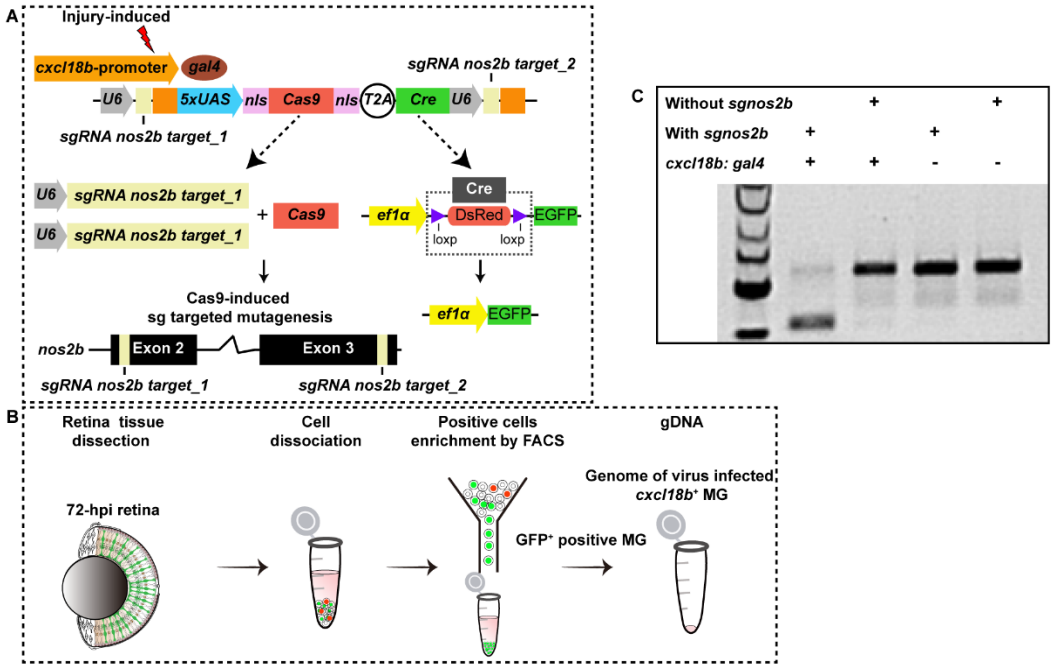

D

virus	clones	mutations	deletions	insertions	ORF shift	KO efficiency
With sgTarget + *cxcl18b: gal4*	26	18 (69.23%)	12 (46.15%)	12 (46.15%)	12 (46.15%)	12 (46.15%)
Without sgTarget + *cxcl18b: gal4*	27	1 (3.70%)	0 (0%)	0 (0%)	0 (0%)	1 (3.70%)
With sgTarget	25	1 (3.70%)	0 (0%)	0 (0%)	0 (0%)	0 (0%)
Without sgTarget	21	1 (3.70%)	0 (0%)	0 (0%)	0 (0%)	0 (0%)

Figure 6-figure supplement 1. Analysis of cell-specific knockout efficiency for *nos2b* in virus-infected clones

(A) Schematic showing the cell-specific gene knockout system design. Injury-induced *cxcl18b* promoter directs the expression of *gal4*, which in combination with the *UAS* element, drives the cell-specific expression of Cas9 and Cre. The *U6* promoter enables the broad expression of sgRNAs targeting *nos2b*, and Cas9 mediates gene knockout within the targeted cells through these sgRNAs. The *ef1α* promoter controls the *loxP-DsRed-loxP-EGFP* reporter system, allowing for the switch from DsRed to EGFP upon Cas9 and Cre activity, and GFP^+ MG clones are identified with successful *nos2b* knockout. This system operates with high specificity via double adenovirus infection.

(B) Schematic showing the procedure of virus-infected clones are sorted and enriched by FACS for further knockout efficiency analysis.

(C) Representative gel electrophoresis image showing *nos2b* deletions in knockout cells compared to controls. Single-virus injections were used to assess Cre system leakage. While minimal Cre system leakage was observed, it did not result in detectable *nos2b* knockout.

(D) Summary table showing the knockout efficiency of each virus-injected clone.

1225 **Supplementary Table S1. sgRNA sequences and genotyping primers, related to STAR**
1226 **Methods.**

sgRNA targets sequences	
Gene symbol	**Primer forward**
nos1 sgRNA target-1	TAATACGACTCACTATAGGCTCCCAGGAAAGAGTCGCGTTTTAGAGCTAGAAATAGC
nos1 sgRNA target-2	TAATACGACTCACTATAGGTCACCAGGCCTGTCAACCGTTTTAGAGCTAGAAATAGC
nos2a sgRNA target-1	TAATACGACTCACTATAGGAGGAACTCGCTTTTGGGGGTTTTAGAGCTAGAAATAGC
nos2a sgRNA target-2	TAATACGACTCACTATAGGTGGCTGGTGCCACCGATGGTTTTAGAGCTAGAAATAGC
nos2b sgRNA target-1	TAATACGACTCACTATAGGAGTATTTCAGAAACACATGTTTTAGAGCTAGAAATAGC
nos2b sgRNA target-2	TAATACGACTCACTATAGGATGTGTTACATCACAGAGGTTTTAGAGCTAGAAATAGC
gsnor sgRNA target-1	TAATACGACTCACTATAGGCCCATGAAGTTCGAGTGAGTTTTAGAGCTAGAAATAGC
gsnor sgRNA target-2	TAATACGACTCACTATAGGTCATCCTGGGTCATGAGGGTTTTAGAGCTAGAAATAGC

1227

Genotyping primers for gene disruption		
Gene symbol	**Primer forward**	**Primer reverse**
nos1-sgTarget-1	ATCGTCTCGGACCTCATCCG	ATAGGTTTTCTATTGCCCTGAGCTC
nos1-sgTarget-2	ATGCGAACGATGCTCGC	ATCCTTCCTATCGATGACCCTCTGG
nos2a-sgTarget-1	ATTACTGTTCTGTCGACTTGATAAACACG	ATACTTAAGATGAGTGCACAAGGCATG
nos2a-sgTarget-2	ATTTAGCCACTCTGAAATTCAAGCC	ATCAGTCCTTTGAAGCTGACCTTGC
nos2b-sgTarget-1	ATTGCAGCACGTTATACTCTCTTAGC	AATGGGCACTGCTTGACTTTAT
nos2b-sgTarget-2	ACTCACAAGAGCGAACTACTGC	ATTGACCCTTCACAAATCTTAGACG
gsnor-sgTarget-1	ATTAATTTTCAGGTGATCAAATGTAAGGC	ATGGGGTGAAGTTGAGTCAGC
gsnor-sgTarget-2	ATGTATTCAAAGTGTGTAATGTAGTCGG	TACCTGATTTTCTGGCACAGG

1228

1229

1230 **Supplementary Table S2. Plasmid construction primer sequences, related to STAR**
1231 **Methods.**

Plasmid construction primer sequences			
Plasmid	**Elements**	**Primer forward**	**Primer reverse**
pTol2-cxcl18b: GFP	*cxcl18b-promoter*	TAGGGCGAATTGGGCATTTGTCTCCTCATGCATTGACTAC	AATTGCTGCAAACTATATGTAGGAAATGCTG
	GFP	ATGGTGAGCAAGGGC	TTACTTGTACAGCTCGTCCATGC
pTol2-cxcl18b: gal4FF	*gal4FF*	ATGAAGCTACTGTCTTCTATCGAACAAGC	CTACCCACCGTACTCGTCAATTCC
pTol2-cxcl18b: Cre-vmhc: mCherry	*Cre*	ATGGCCAATTTACTGACCGTACACC	CTAATCGCCATCTTCCAGCAGGC
	vmhc: mCherry	CATGTGTCCTAAATTCTGAAAACACAGTAAGCC	TTACTTGTACAGCTCGTCCATG
pTol2-UAS: Cas9-T2A-Cre-U6: nos2b sgRNA1; U6: nos2b sgRNA2	*nos2b sgRNA1*	CTCGGGTCGCTCTTGTGAGTGACC	AAACGGTCACTCACAAGAGCGACC
	nos2b sgRNA2	AGCTCGGGCTGGTGCCGCCAATGTCG	TAAACGACATTGGCGGCACCAGCCCG

1232
1233

1234 **Supplementary Table S3. qPCR primer sequences, related to STAR Methods.**

Gene symbol	Primer forward	Primer reverse
cxcl18b	TGCTGCTCGCGGTAGTTTAC	TCTGCAGTAATTGGCCCTGC
glula	CGCATTACAGAGCCTGCCTA	ATTCCAGTTGCCTGGGATCG
glulb	ATGGTCCAGAACCAGCATCC	TCACAAGGGCCAACTTGGAA
pcna	CAGAAACCTAGCCATGGGGG	GTCTTGGACAGAGGAGTGGC
nos1	TGAGCACGTTTGCATAGGGT	CACTGGATTCGTCCCACACA
nos2a	CCAGATAACCACTGCTCTGCT	CTTGTCTTCCCATCTTGCTAAAA
nos2b	GAGGCAAAATTCCACCACCAG	TGCAAAGTGGTCATGGGACA
gsnor	ACAAGAAATCTCCACCCGGC	GACGGCTCGGATACTCTTCC
β-actin	ATTGCTGACAGGATGCAGAAG	GATGGTCCAGACTCATCGTACTC

1235

1236

Reference: Uncategorized References

Abalo, X.M., Lagman, D., Heras, G., Del Pozo, A., Eggert, J., and Larhammar, D. (2020). Circadian regulation of phosphodiesterase 6 genes in zebrafish differs between cones and rods: Implications for photopic and scotopic vision. Vision research *166*, 43-51.

Abraham, E., Hartmann, H., Yoshimatsu, T., Baden, T., and Brand, M. (2024). Restoration of cone-circuit functionality in the regenerating adult zebrafish retina. Developmental cell *59*, 2158-2170.e2156.

Asaoka, Y., Hata, S., Namae, M., Furutani-Seiki, M., and Nishina, H. (2014). The Hippo pathway controls a switch between retinal progenitor cell proliferation and photoreceptor cell differentiation in zebrafish. PloS one *9*, e97365.

Ashpole, N.M., Chawla, A.R., Martin, M.P., Brustovetsky, T., Brustovetsky, N., and Hudmon, A. (2013). Loss of calcium/calmodulin-dependent protein kinase II activity in cortical astrocytes decreases glutamate uptake and induces neurotoxic release of ATP. The Journal of biological chemistry *288*, 14599-14611.

Ashpole, N.M., Song, W., Brustovetsky, T., Engleman, E.A., Brustovetsky, N., Cummins, T.R., and Hudmon, A. (2012). Calcium/calmodulin-dependent protein kinase II (CaMKII) inhibition induces neurotoxicity via dysregulation of glutamate/calcium signaling and hyperexcitability. The Journal of biological chemistry *287*, 8495-8506.

Bedi, O., Sapra, V., Kumar, M., and Krishan, P. (2024). Newer mitochondrial dynamics and their role of calcium signalling in liver regeneration. Mitochondrion *79*, 101969.

Bernardos, R.L., and Raymond, P.A. (2006). GFAP transgenic zebrafish. Gene expression patterns : GEP *6*, 1007-1013.

Boyd, P., Campbell, L.J., and Hyde, D.R. (2023). Clcf1/Crlf1a-mediated signaling is neuroprotective and required for Müller glia proliferation in the light-damaged zebrafish retina. Frontiers in cell and developmental biology *11*, 1142586.

Bradley, S., Tossell, K., Lockley, R., and McDearmid, J.R. (2010). Nitric oxide synthase regulates morphogenesis of zebrafish spinal cord motoneurons. The Journal of neuroscience : the official journal of the Society for Neuroscience *30*, 16818-16831.

Breus, O., and Dickmeis, T. (2021). Genetically encoded thiol redox-sensors in the zebrafish model: lessons for embryonic development and regeneration. Biological chemistry *402*, 363-378.

Campbell, L.J., Hobgood, J.S., Jia, M., Boyd, P., Hipp, R.I., and Hyde, D.R. (2021). Notch3 and DeltaB maintain Müller glia quiescence and act as negative regulators of regeneration in the light-damaged zebrafish retina. Glia *69*, 546-566.

Campbell, L.J., Levendusky, J.L., Steines, S.A., and Hyde, D.R. (2022). Retinal regeneration requires dynamic Notch signaling. Neural regeneration research *17*, 1199-1209.

Celotto, L., Rost, F., Machate, A., Bläsche, J., Dahl, A., Weber, A., Hans, S., and Brand, M. (2023). Single-cell RNA sequencing unravels the transcriptional network

underlying zebrafish retina regeneration. eLife *12*.
Charles, N., Ozawa, T., Squatrito, M., Bleau, A.M., Brennan, C.W., Hambardzumyan, D., and Holland, E.C. (2010). Perivascular nitric oxide activates notch signaling and promotes stem-like character in PDGF-induced glioma cells. Cell stem cell *6*, 141-152.
Close, J.L., Gumuscu, B., and Reh, T.A. (2005). Retinal neurons regulate proliferation of postnatal progenitors and Müller glia in the rat retina via TGF beta signaling. Development (Cambridge, England) *132*, 3015-3026.
Close, J.L., Liu, J., Gumuscu, B., and Reh, T.A. (2006). Epidermal growth factor receptor expression regulates proliferation in the postnatal rat retina. Glia *54*, 94-104.
Conner, C., Ackerman, K.M., Lahne, M., Hobgood, J.S., and Hyde, D.R. (2014). Repressing notch signaling and expressing TNFα are sufficient to mimic retinal regeneration by inducing Müller glial proliferation to generate committed progenitor cells. The Journal of neuroscience : the official journal of the Society for Neuroscience *34*, 14403-14419.
Curado, S., Anderson, R.M., Jungblut, B., Mumm, J., Schroeter, E., and Stainier, D.Y. (2007). Conditional targeted cell ablation in zebrafish: a new tool for regeneration studies. Developmental dynamics : an official publication of the American Association of Anatomists *236*, 1025-1035.
Curado, S., Stainier, D.Y., and Anderson, R.M. (2008). Nitroreductase-mediated cell/tissue ablation in zebrafish: a spatially and temporally controlled ablation method with applications in developmental and regeneration studies. Nature protocols *3*, 948-954.
Dermietzel, R., Kremer, M., Paputsoglu, G., Stang, A., Skerrett, I.M., Gomes, D., Srinivas, M., Janssen-Bienhold, U., Weiler, R., Nicholson, B.J.*, et al.* (2000). Molecular and functional diversity of neural connexins in the retina. The Journal of neuroscience : the official journal of the Society for Neuroscience *20*, 8331-8343.
Di Donato, V., De Santis, F., Auer, T.O., Testa, N., Sánchez-Iranzo, H., Mercader, N., Concordet, J.P., and Del Bene, F. (2016). 2C-Cas9: a versatile tool for clonal analysis of gene function. Genome research *26*, 681-692.
Ellett, F., Pase, L., Hayman, J.W., Andrianopoulos, A., and Lieschke, G.J. (2011). mpeg1 promoter transgenes direct macrophage-lineage expression in zebrafish. Blood *117*, e49-56.
Fausett, B.V., Gumerson, J.D., and Goldman, D. (2008). The proneural basic helix-loop-helix gene ascl1a is required for retina regeneration. The Journal of neuroscience : the official journal of the Society for Neuroscience *28*, 1109-1117.
Förstermann, U., and Sessa, W.C. (2012). Nitric oxide synthases: regulation and function. European heart journal *33*, 829-837, 837a-837d.
Gao, H., A, L., Huang, X., Chen, X., and Xu, H. (2021). Müller Glia-Mediated Retinal Regeneration. Molecular neurobiology *58*, 2342-2361.
Goldman, D. (2014). Müller glial cell reprogramming and retina regeneration. Nature reviews Neuroscience *15*, 431-442.
Goldstein, S., Russo, A., and Samuni, A. (2003). Reactions of PTIO and carboxy-PTIO with *NO, *NO2, and O2-*. The Journal of biological chemistry *278*, 50949-

50955.
Gonzalez-Nunez, V., Nocco, V., and Budd, A. (2010). Characterization of drCol 15a1b: a novel component of the stem cell niche in the zebrafish retina. Stem cells (Dayton, Ohio) *28*, 1399-1411.
Gorsuch, R.A., Lahne, M., Yarka, C.E., Petravick, M.E., Li, J., and Hyde, D.R. (2017). Sox2 regulates Müller glia reprogramming and proliferation in the regenerating zebrafish retina via Lin28 and Ascl1a. Experimental eye research *161*, 174-192.
Goumenaki, P., Günther, S., Kikhi, K., Looso, M., Marín-Juez, R., and Stainier, D.Y.R. (2024). The innate immune regulator MyD88 dampens fibrosis during zebrafish heart regeneration. Nature cardiovascular research *3*, 1158-1176.
Grover, L.M., and Teyler, T.J. (1990). Two components of long-term potentiation induced by different patterns of afferent activation. Nature *347*, 477-479.
Han, P., Zhou, X.H., Chang, N., Xiao, C.L., Yan, S., Ren, H., Yang, X.Z., Zhang, M.L., Wu, Q., Tang, B.*, et al.* (2014). Hydrogen peroxide primes heart regeneration with a derepression mechanism. Cell research *24*, 1091-1107.
Hans, S., Kaslin, J., Freudenreich, D., and Brand, M. (2009). Temporally-controlled site-specific recombination in zebrafish. PloS one *4*, e4640.
Hanson, Q.M., Carley, J.R., Gilbreath, T.J., Smith, B.C., and Underbakke, E.S. (2018). Calmodulin-induced Conformational Control and Allostery Underlying Neuronal Nitric Oxide Synthase Activation. Journal of molecular biology *430*, 935-947.
Hoang, T., Wang, J., Boyd, P., Wang, F., Santiago, C., Jiang, L., Yoo, S., Lahne, M., Todd, L.J., Jia, M.*, et al.* (2020). Gene regulatory networks controlling vertebrate retinal regeneration. Science (New York, NY) *370*.
Hong, J., Kim, B.K., Lim, H., Lee, S., and Lee, S.J. (2012). Identification and characterization of triamcinolone acetonide, a microglial-activation inhibitor. Immunopharmacology and immunotoxicology *34*, 912-918.
Hunter, M.V., Willoughby, P.M., Bruce, A.E.E., and Fernandez-Gonzalez, R. (2018). Oxidative Stress Orchestrates Cell Polarity to Promote Embryonic Wound Healing. Developmental cell *47*, 377-387.e374.
Iribarne, M., and Hyde, D.R. (2022). Different inflammation responses modulate Müller glia proliferation in the acute or chronically damaged zebrafish retina. Frontiers in cell and developmental biology *10*, 892271.
Jaeschke, H. (2000). Reactive oxygen and mechanisms of inflammatory liver injury. Journal of gastroenterology and hepatology *15*, 718-724.
Janssen-Bienhold, U., Dermietzel, R., and Weiler, R. (1998). Distribution of connexin43 immunoreactivity in the retinas of different vertebrates. The Journal of comparative neurology *396*, 310-321.
Jia, W., Channappanavar, R., Zhang, C., Li, M., Zhou, H., Zhang, S., Zhou, P., Xu, J., Shan, S., Shi, X.*, et al.* (2019). Single intranasal immunization with chimpanzee adenovirus-based vaccine induces sustained and protective immunity against MERS-CoV infection. Emerging microbes & infections *8*, 760-772.
Jones, R.J., Jourd'heuil, D., Salerno, J.C., Smith, S.M., and Singer, H.A. (2007). iNOS regulation by calcium/calmodulin-dependent protein kinase II in vascular

1368 smooth muscle. American journal of physiology Heart and circulatory physiology *292*,
1369 H2634-2642.
1370 Jorstad, N.L., Wilken, M.S., Grimes, W.N., Wohl, S.G., VandenBosch, L.S.,
1371 Yoshimatsu, T., Wong, R.O., Rieke, F., and Reh, T.A. (2017). Stimulation of functional
1372 neuronal regeneration from Müller glia in adult mice. Nature *548*, 103-107.
1373 Kawamoto, E.M., Vivar, C., and Camandola, S. (2012). Physiology and pathology of
1374 calcium signaling in the brain. Frontiers in pharmacology *3*, 61.
1375 Kimura, M., Moteki, H., and Ogihara, M. (2023). Role of Hepatocyte Growth
1376 Regulators in Liver Regeneration. Cells *12*.
1377 Krylov, A., Yu, S., Veen, K., Newton, A., Ye, A., Qin, H., He, J., and Jusuf, P.R. (2023).
1378 Heterogeneity in quiescent Müller glia in the uninjured zebrafish retina drive
1379 differential responses following photoreceptor ablation. Frontiers in molecular
1380 neuroscience *16*, 1087136.
1381 Kwan, K.M., Fujimoto, E., Grabher, C., Mangum, B.D., Hardy, M.E., Campbell, D.S.,
1382 Parant, J.M., Yost, H.J., Kanki, J.P., and Chien, C.B. (2007). The Tol2kit: a multisite
1383 gateway-based construction kit for Tol2 transposon transgenesis constructs.
1384 Developmental dynamics : an official publication of the American Association of
1385 Anatomists *236*, 3088-3099.
1386 Kyritsis, N., Kizil, C., Zocher, S., Kroehne, V., Kaslin, J., Freudenreich, D., Iltzsche,
1387 A., and Brand, M. (2012). Acute inflammation initiates the regenerative response in
1388 the adult zebrafish brain. Science (New York, NY) *338*, 1353-1356.
1389 Lahne, M., Brecker, M., Jones, S.E., and Hyde, D.R. (2020a). The Regenerating
1390 Adult Zebrafish Retina Recapitulates Developmental Fate Specification Programs.
1391 Frontiers in cell and developmental biology *8*, 617923.
1392 Lahne, M., Nagashima, M., Hyde, D.R., and Hitchcock, P.F. (2020b). Reprogramming
1393 Müller Glia to Regenerate Retinal Neurons. Annual review of vision science *6*, 171-
1394 193.
1395 Leach, L.L., Hanovice, N.J., George, S.M., Gabriel, A.E., and Gross, J.M. (2021). The
1396 immune response is a critical regulator of zebrafish retinal pigment epithelium
1397 regeneration. Proceedings of the National Academy of Sciences of the United States
1398 of America *118*.
1399 Lee, M.S., Jui, J., Sahu, A., and Goldman, D. (2024). Mycb and Mych stimulate
1400 Müller glial cell reprogramming and proliferation in the uninjured and injured zebrafish
1401 retina. Development (Cambridge, England) *151*.
1402 Lee, M.S., Wan, J., and Goldman, D. (2020). Tgfb3 collaborates with PP2A and notch
1403 signaling pathways to inhibit retina regeneration. eLife *9*.
1404 Lenkowski, J.R., and Raymond, P.A. (2014). Müller glia: Stem cells for generation
1405 and regeneration of retinal neurons in teleost fish. Progress in retinal and eye
1406 research *40*, 94-123.
1407 Levin, M. (2009). Bioelectric mechanisms in regeneration: Unique aspects and future
1408 perspectives. Seminars in cell & developmental biology *20*, 543-556.
1409 Liu, J., Xu, K., Xing, M., Zhuo, Y., Guo, J., Du, M., Wang, Q., An, Y., Li, J., Gao, P.*, et*
1410 *al.* (2021). Heterologous prime-boost immunizations with chimpanzee adenoviral
1411 vectors elicit potent and protective immunity against SARS-CoV-2 infection. Cell

1412 discovery *7*, 123.
1413 López-Juárez, A., Titus, H.E., Silbak, S.H., Pressler, J.W., Rizvi, T.A., Bogard, M.,
1414 Bennett, M.R., Ciraolo, G., Williams, M.T., Vorhees, C.V.*, et al.* (2017).
1415 Oligodendrocyte Nf1 Controls Aberrant Notch Activation and Regulates Myelin
1416 Structure and Behavior. Cell reports *19*, 545-557.
1417 Lu, C., and Hyde, D.R. (2024). Cytokines IL-1β and IL-10 are required for Müller glia
1418 proliferation following light damage in the adult zebrafish retina. Frontiers in cell and
1419 developmental biology *12*, 1406330.
1420 Lyu, P., Iribarne, M., Serjanov, D., Zhai, Y., Hoang, T., Campbell, L.J., Boyd, P.,
1421 Palazzo, I., Nagashima, M., Silva, N.J.*, et al.* (2023). Common and divergent gene
1422 regulatory networks control injury-induced and developmental neurogenesis in
1423 zebrafish retina. Nat Commun *14*, 8477.
1424 Matrone, G., Jung, S.Y., Choi, J.M., Jain, A., Leung, H.E., Rajapakshe, K., Coarfa,
1425 C., Rodor, J., Denvir, M.A., Baker, A.H.*, et al.* (2021). Nuclear S-nitrosylation impacts
1426 tissue regeneration in zebrafish. Nat Commun *12*, 6282.
1427 Moore, P.K., al-Swayeh, O.A., Chong, N.W., Evans, R.A., and Gibson, A. (1990). L-
1428 NG-nitro arginine (L-NOARG), a novel, L-arginine-reversible inhibitor of endothelium-
1429 dependent vasodilatation in vitro. British journal of pharmacology *99*, 408-412.
1430 Nelson, C.M., Ackerman, K.M., O'Hayer, P., Bailey, T.J., Gorsuch, R.A., and Hyde,
1431 D.R. (2013). Tumor necrosis factor-alpha is produced by dying retinal neurons and is
1432 required for Muller glia proliferation during zebrafish retinal regeneration. The Journal
1433 of neuroscience : the official journal of the Society for Neuroscience *33*, 6524-6539.
1434 Nishino, R., Nomura-Komoike, K., Iida, T., and Fujieda, H. (2023). Cell cycle-
1435 dependent activation of proneural transcription factor expression and reactive gliosis
1436 in rat Müller glia. Scientific reports *13*, 22712.
1437 Pacher, P., Beckman, J.S., and Liaudet, L. (2007). Nitric oxide and peroxynitrite in
1438 health and disease. Physiological reviews *87*, 315-424.
1439 Park, M. (2018). AMPA Receptor Trafficking for Postsynaptic Potentiation. Frontiers
1440 in cellular neuroscience *12*, 361.
1441 Parsons, M.J., Pisharath, H., Yusuff, S., Moore, J.C., Siekmann, A.F., Lawson, N.,
1442 and Leach, S.D. (2009). Notch-responsive cells initiate the secondary transition in
1443 larval zebrafish pancreas. Mechanisms of development *126*, 898-912.
1444 Picelli, S., Björklund Å, K., Faridani, O.R., Sagasser, S., Winberg, G., and Sandberg,
1445 R. (2013). Smart-seq2 for sensitive full-length transcriptome profiling in single cells.
1446 Nature methods *10*, 1096-1098.
1447 Powell, C., Cornblath, E., Elsaeidi, F., Wan, J., and Goldman, D. (2016). Zebrafish
1448 Müller glia-derived progenitors are multipotent, exhibit proliferative biases and
1449 regenerate excess neurons. Scientific reports *6*, 24851.
1450 Qin, C., Qi, Z., Pan, S., Xia, P., Kong, W., Sun, B., Du, H., Zhang, R., Zhu, L., Zhou,
1451 D.*, et al.* (2023). Advances in Conductive Hydrogel for Spinal Cord Injury Repair and
1452 Regeneration. International journal of nanomedicine *18*, 7305-7333.
1453 Quillien, A., Moore, J.C., Shin, M., Siekmann, A.F., Smith, T., Pan, L., Moens, C.B.,
1454 Parsons, M.J., and Lawson, N.D. (2014). Distinct Notch signaling outputs pattern the
1455 developing arterial system. Development (Cambridge, England) *141*, 1544-1552.

1456 Ramachandran, R., Fausett, B.V., and Goldman, D. (2010). Ascl1a regulates Müller
1457 glia dedifferentiation and retinal regeneration through a Lin-28-dependent, let-7
1458 microRNA signalling pathway. Nature cell biology *12*, 1101-1107.
1459 Raymond, P.A., Barthel, L.K., Bernardos, R.L., and Perkowski, J.J. (2006). Molecular
1460 characterization of retinal stem cells and their niches in adult zebrafish. BMC
1461 developmental biology *6*, 36.
1462 Rees, D.D., Palmer, R.M., Schulz, R., Hodson, H.F., and Moncada, S. (1990).
1463 Characterization of three inhibitors of endothelial nitric oxide synthase in vitro and in
1464 vivo. British journal of pharmacology *101*, 746-752.
1465 Rochon, E.R., Missinato, M.A., Xue, J., Tejero, J., Tsang, M., Gladwin, M.T., and
1466 Corti, P. (2020). Nitrite Improves Heart Regeneration in Zebrafish. Antioxidants &
1467 redox signaling *32*, 363-377.
1468 Sahu, A., Devi, S., Jui, J., and Goldman, D. (2021). Notch signaling via Hey1 and
1469 Id2b regulates Müller glia's regenerative response to retinal injury. Glia *69*, 2882-
1470 2898.
1471 Shen, Y.C., and Raymond, P.A. (2004). Zebrafish cone-rod (crx) homeobox gene
1472 promotes retinogenesis. Developmental biology *269*, 237-251.
1473 Silva, N.J., Nagashima, M., Li, J., Kakuk-Atkins, L., Ashrafzadeh, M., Hyde, D.R., and
1474 Hitchcock, P.F. (2020). Inflammation and matrix metalloproteinase 9 (Mmp-9)
1475 regulate photoreceptor regeneration in adult zebrafish. Glia *68*, 1445-1465.
1476 Tang, X., Gao, J., Jia, X., Zhao, W., Zhang, Y., Pan, W., and He, J. (2017). Bipotent
1477 progenitors as embryonic origin of retinal stem cells. The Journal of cell biology *216*,
1478 1833-1847.
1479 Thummel, R., Kassen, S.C., Enright, J.M., Nelson, C.M., Montgomery, J.E., and
1480 Hyde, D.R. (2008). Characterization of Müller glia and neuronal progenitors during
1481 adult zebrafish retinal regeneration. Experimental eye research *87*, 433-444.
1482 Torraca, V., Otto, N.A., Tavakoli-Tameh, A., and Meijer, A.H. (2017). The inflammatory
1483 chemokine Cxcl18b exerts neutrophil-specific chemotaxis via the promiscuous
1484 chemokine receptor Cxcr2 in zebrafish. Developmental and comparative immunology
1485 *67*, 57-65.
1486 Vihtelic, T.S., and Hyde, D.R. (2000). Light-induced rod and cone cell death and
1487 regeneration in the adult albino zebrafish (Danio rerio) retina. Journal of neurobiology
1488 *44*, 289-307.
1489 Villegas, S.N., Gombos, R., García-López, L., Gutiérrez-Pérez, I., García-Castillo, J.,
1490 Vallejo, D.M., Da Ros, V.G., Ballesta-Illán, E., Mihály, J., and Dominguez, M. (2018).
1491 PI3K/Akt Cooperates with Oncogenic Notch by Inducing Nitric Oxide-Dependent
1492 Inflammation. Cell reports *22*, 2541-2549.
1493 Wan, J., and Goldman, D. (2016). Retina regeneration in zebrafish. Current opinion
1494 in genetics & development *40*, 41-47.
1495 Wan, J., and Goldman, D. (2017). Opposing Actions of Fgf8a on Notch Signaling
1496 Distinguish Two Muller Glial Cell Populations that Contribute to Retina Growth and
1497 Regeneration. Cell reports *19*, 849-862.
1498 Wan, J., Ramachandran, R., and Goldman, D. (2012). HB-EGF is necessary and
1499 sufficient for Müller glia dedifferentiation and retina regeneration. Developmental cell

22, 334-347.
Wang, H., Yang, Z., Li, X., Huang, D., Yu, S., He, J., Li, Y., and Yan, J. (2020). Single-cell in vivo imaging of cellular circadian oscillators in zebrafish. PLoS biology *18*, e3000435.
White, D.T., Sengupta, S., Saxena, M.T., Xu, Q., Hanes, J., Ding, D., Ji, H., and Mumm, J.S. (2017). Immunomodulation-accelerated neuronal regeneration following selective rod photoreceptor cell ablation in the zebrafish retina. Proceedings of the National Academy of Sciences of the United States of America *114*, E3719-e3728.
Wu, D.M., Schneiderman, T., Burgett, J., Gokhale, P., Barthel, L., and Raymond, P.A. (2001). Cones regenerate from retinal stem cells sequestered in the inner nuclear layer of adult goldfish retina. Investigative ophthalmology & visual science *42*, 2115-2124.
Wu, R.S., Lam, II, Clay, H., Duong, D.N., Deo, R.C., and Coughlin, S.R. (2018). A Rapid Method for Directed Gene Knockout for Screening in G0 Zebrafish. Developmental cell *46*, 112-125.e114.
Xiao, X., Liao, Z., and Zou, J. (2023). Genetic and epigenetic regulators of retinal Müller glial cell reprogramming. Advances in ophthalmology practice and research *3*, 126-133.
Xu, B., Tang, X., Jin, M., Zhang, H., Du, L., Yu, S., and He, J. (2020). Unifying developmental programs for embryonic and postembryonic neurogenesis in the zebrafish retina. Development (Cambridge, England) *147*.
Yeo, S.Y., Kim, M., Kim, H.S., Huh, T.L., and Chitnis, A.B. (2007). Fluorescent protein expression driven by her4 regulatory elements reveals the spatiotemporal pattern of Notch signaling in the nervous system of zebrafish embryos. Developmental biology *301*, 555-567.
Yoo, S.K., Freisinger, C.M., LeBert, D.C., and Huttenlocher, A. (2012). Early redox, Src family kinase, and calcium signaling integrate wound responses and tissue regeneration in zebrafish. The Journal of cell biology *199*, 225-234.
Yu, C., Li, X., Ma, J., Liang, S., Zhao, Y., Li, Q., and Zhang, R. (2024). Spatiotemporal modulation of nitric oxide and Notch signaling by hemodynamic-responsive Trpv4 is essential for ventricle regeneration. Cellular and molecular life sciences : CMLS *81*, 60.
Yu, S., and He, J. (2019). Stochastic cell-cycle entry and cell-state-dependent fate outputs of injury-reactivated tectal radial glia in zebrafish. eLife *8*.
Yurco, P., and Cameron, D.A. (2005). Responses of Müller glia to retinal injury in adult zebrafish. Vision research *45*, 991-1002.
Zhang, H., Hao, J., Hong, H., Gu, W., Li, Z., Sun, J., Zhan, H., Wei, X., and Zhou, L. (2024). Redox signaling regulates the skeletal tissue development and regeneration. Biotechnology & genetic engineering reviews *40*, 2308-2331.
Zhang, Z., Hou, H., Yu, S., Zhou, C., Zhang, X., Li, N., Zhang, S., Song, K., Lu, Y., Liu, D.*, et al.* (2020). Inflammation-induced mammalian target of rapamycin signaling is essential for retina regeneration. Glia *68*, 111-127.

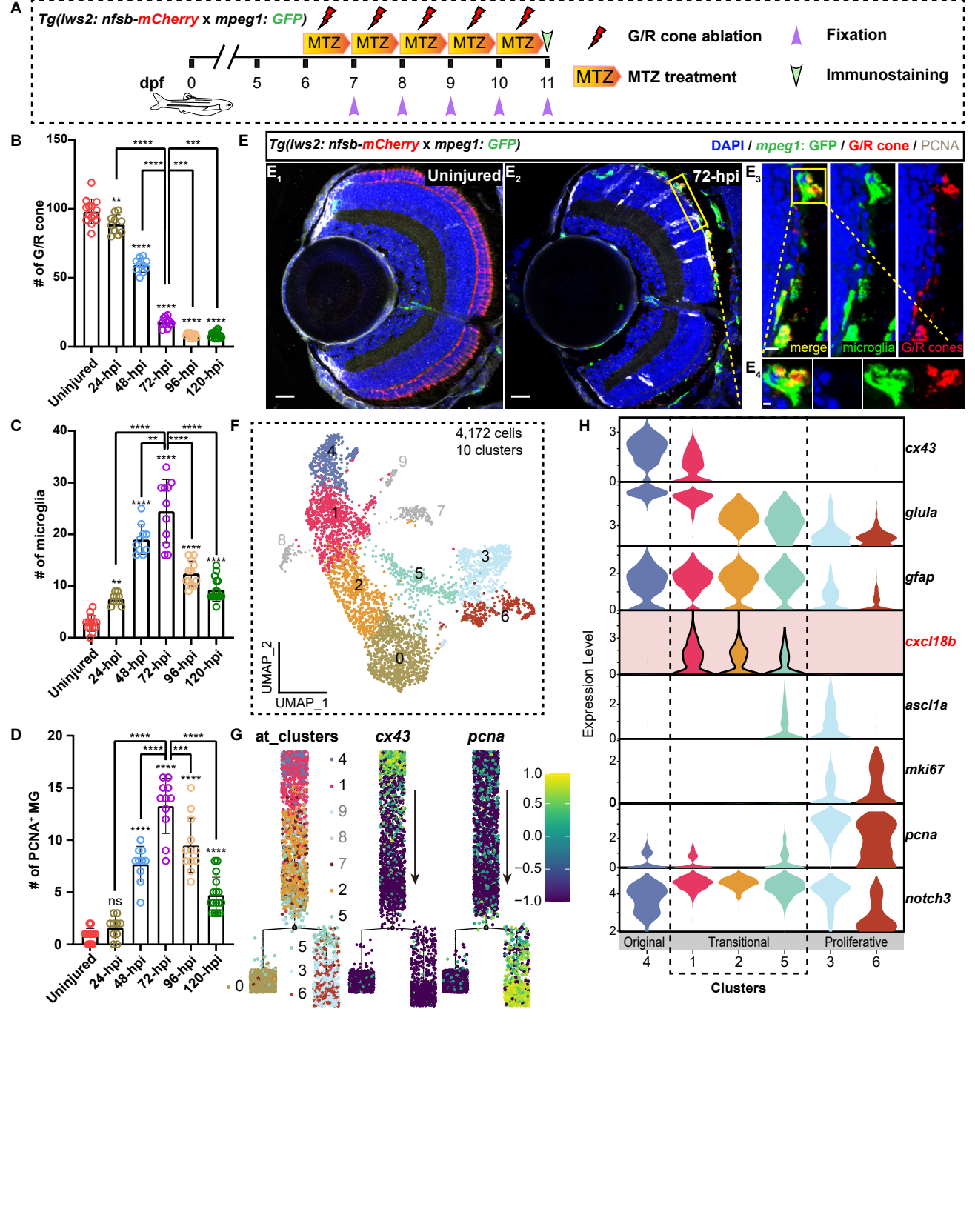
A
Tg(lws2: nfsb-mCherry x mpeg1: GFP)
MTZ
dpf
0
5
6
7
8
9
10
11
G/R cone ablation
MTZ treatment
Fixation
Immunostaining
B
# of G/R cone
Uninjured
24-hpi
48-hpi
72-hpi
96-hpi
120-hpi
E
Tg(lws2: nfsb-mCherry x mpeg1: GFP)
DAPI / mpeg1: GFP / G/R cone / PCNA
Uninjured
72-hpi
merge
microglia
G/R cones
C
# of microglia
F
4,172 cells
10 clusters
UMAP_2
UMAP_1
H
cx43
glula
gfap
cxcl18b
ascl1a
mki67
pcna
notch3
Expression Level
Original
Transitional
Proliferative
Clusters
D
# of PCNA+ MG
ns
G
at_clusters
cx43
pcna

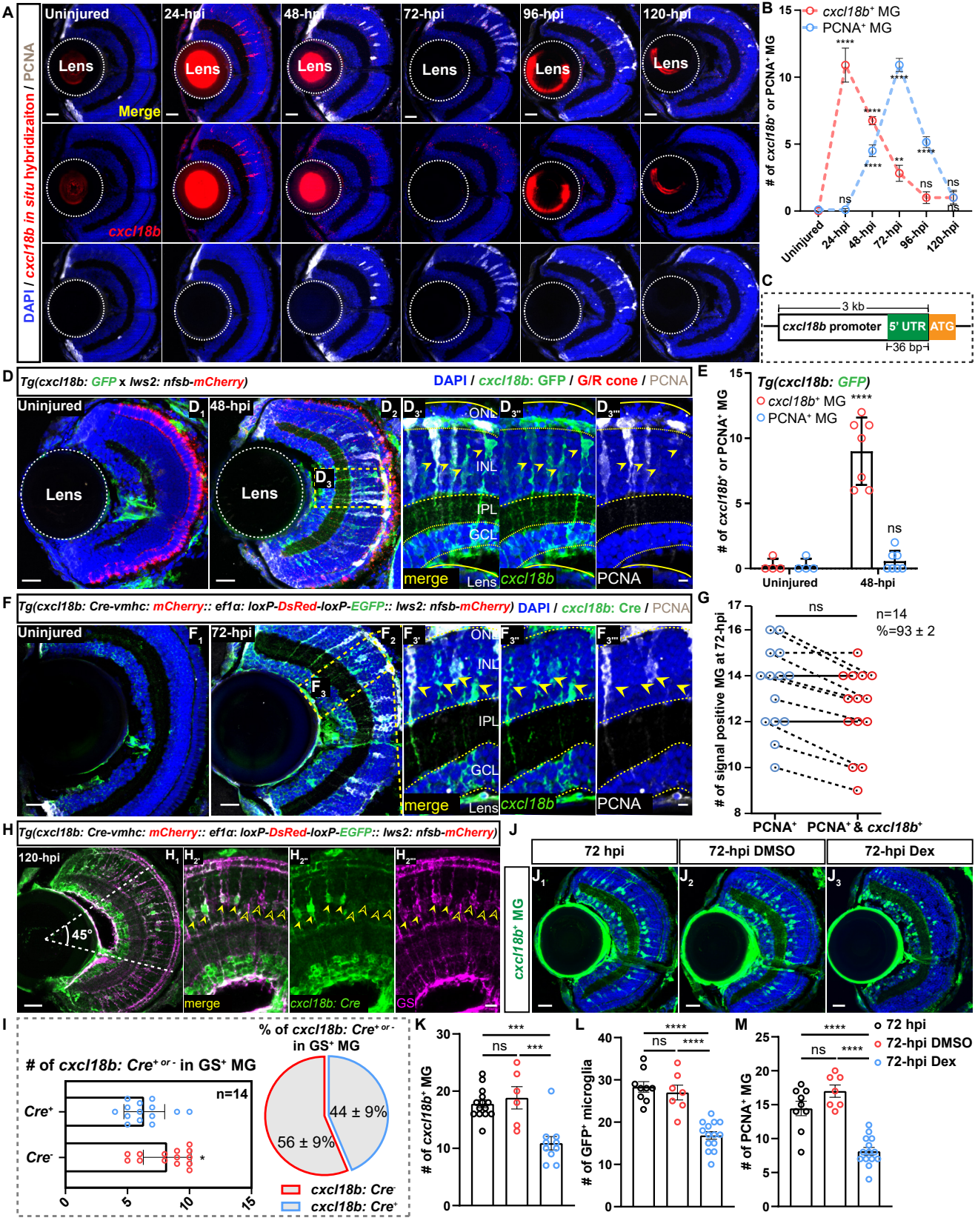
A
DAPI / cxcl18b in situ hybridizaiton / PCNA
Uninjured
24-hpi
48-hpi
72-hpi
96-hpi
120-hpi
Lens
Merge
cxcl18b
B
cxcl18b+ MG
PCNA+ MG
# of cxcl18b+ or PCNA+ MG
Uninjured
24-hpi
48-hpi
72-hpi
96-hpi
120-hpi
C
3 kb
cxcl18b promoter
5' UTR
ATG
36 bp
D
Tg(cxcl18b: GFP x lws2: nfsb-mCherry)
DAPI / cxcl18b: GFP / G/R cone / PCNA
Uninjured
48-hpi
Lens
ONL
INL
IPL
GCL
merge
cxcl18b
PCNA
E
Tg(cxcl18b: GFP)
cxcl18b+ MG
PCNA+ MG
# of cxcl18b+ or PCNA+ MG
Uninjured
48-hpi
ns
F
Tg(cxcl18b: Cre-vmhc: mCherry:: ef1α: loxP-DsRed-loxP-EGFP:: lws2: nfsb-mCherry)
DAPI / cxcl18b: Cre / PCNA
Uninjured
72-hpi
ONL
INL
IPL
GCL
merge
cxcl18b
PCNA
G
ns
n=14
%=93 ± 2
# of signal positive MG at 72-hpi
PCNA+
PCNA+ & cxcl18b+
H
Tg(cxcl18b: Cre-vmhc: mCherry:: ef1α: loxP-DsRed-loxP-EGFP:: lws2: nfsb-mCherry)
120-hpi
45°
merge
cxcl18b: Cre
GS
J
72 hpi
72-hpi DMSO
72-hpi Dex
cxcl18b+ MG
I
# of cxcl18b: Cre+ or - in GS+ MG
n=14
Cre+
Cre-
% of cxcl18b: Cre+ or - in GS+ MG
44 ± 9%
56 ± 9%
cxcl18b: Cre-
cxcl18b: Cre+
K
# of cxcl18b+ MG
ns
L
# of GFP+ microglia
ns
M
# of PCNA+ MG
ns
72 hpi
72-hpi DMSO
72-hpi Dex

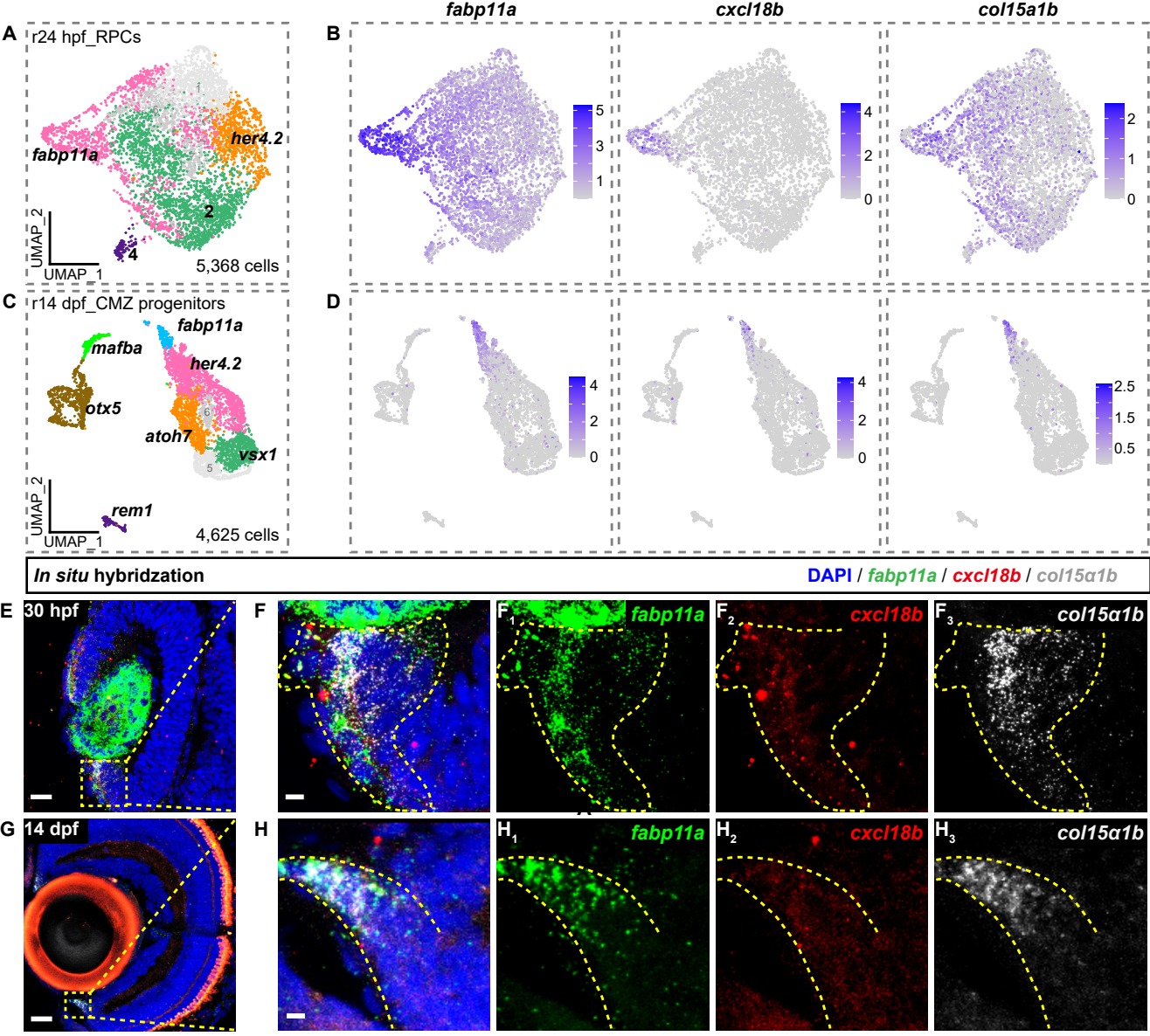
fabp11a
cxcl18b
col15a1b
A
r24 hpf_RPCs
fabp11a
her4.2
2
4
UMAP_2
UMAP_1
5,368 cells
B
C
r14 dpf_CMZ progenitors
fabp11a
mafba
her4.2
otx5
atoh7
vsx1
rem1
4,625 cells
D
In situ hybridzation
DAPI / fabp11a / cxcl18b / col15a1b
E
30 hpf
F
F1
fabp11a
F2
cxcl18b
F3
col15a1b
G
14 dpf
H
H1
fabp11a
H2
cxcl18b
H3
col15a1b

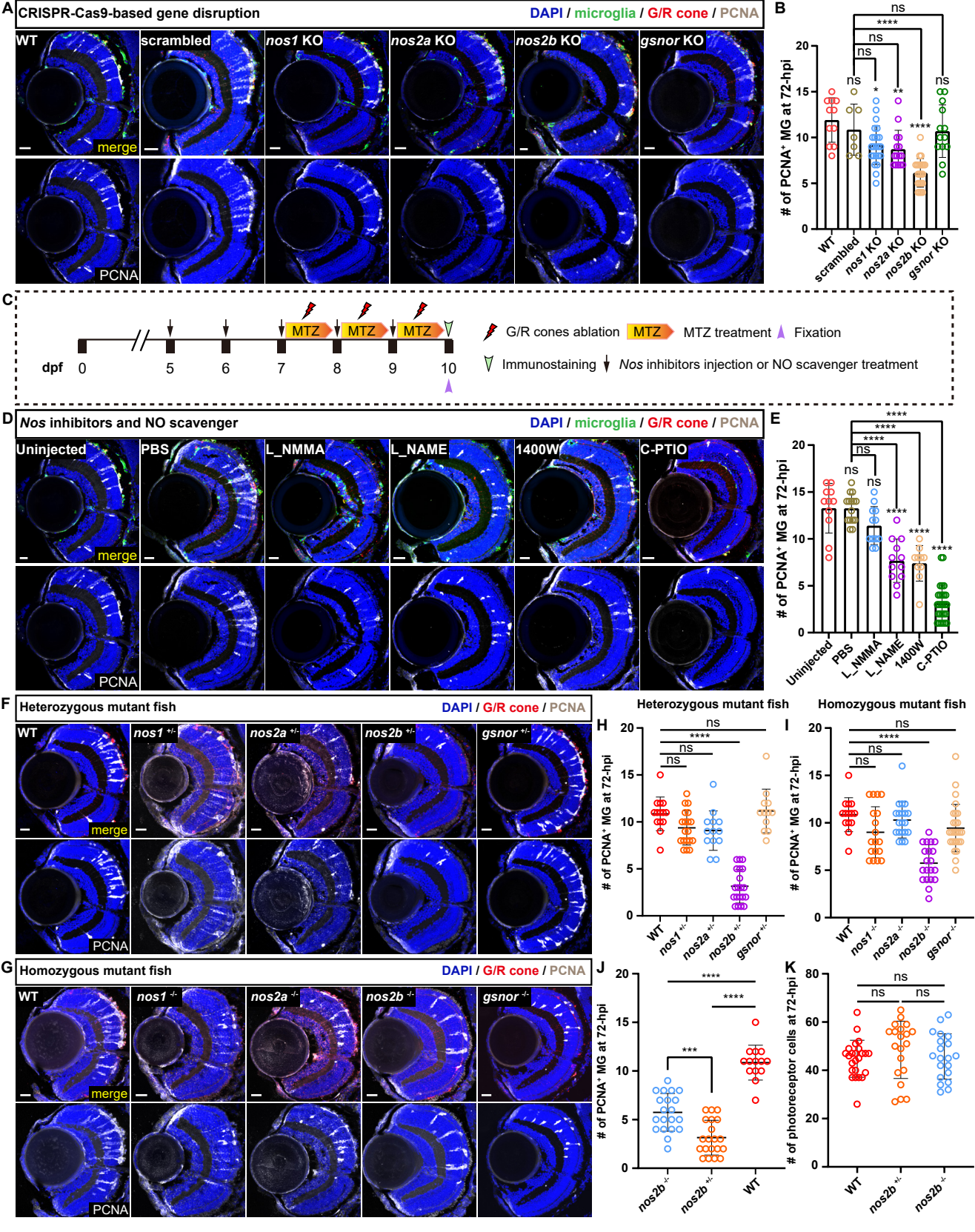
A
CRISPR-Cas9-based gene disruption
DAPI / microglia / G/R cone / PCNA
WT
scrambled
nos1 KO
nos2a KO
nos2b KO
gsnor KO
merge
PCNA
B
# of PCNA+ MG at 72-hpi
ns
****
*
**
C
dpf
0
5
6
7
8
9
10
MTZ
G/R cones ablation
MTZ treatment
Fixation
Immunostaining
Nos inhibitors injection or NO scavenger treatment
D
Nos inhibitors and NO scavenger
Uninjected
PBS
L_NMMA
L_NAME
1400W
C-PTIO
E
F
Heterozygous mutant fish
nos1 +/-
nos2a +/-
nos2b +/-
gsnor +/-
G
Homozygous mutant fish
nos1 -/-
nos2a -/-
nos2b -/-
gsnor -/-
H
I
J
K
# of photoreceptor cells at 72-hpi
***

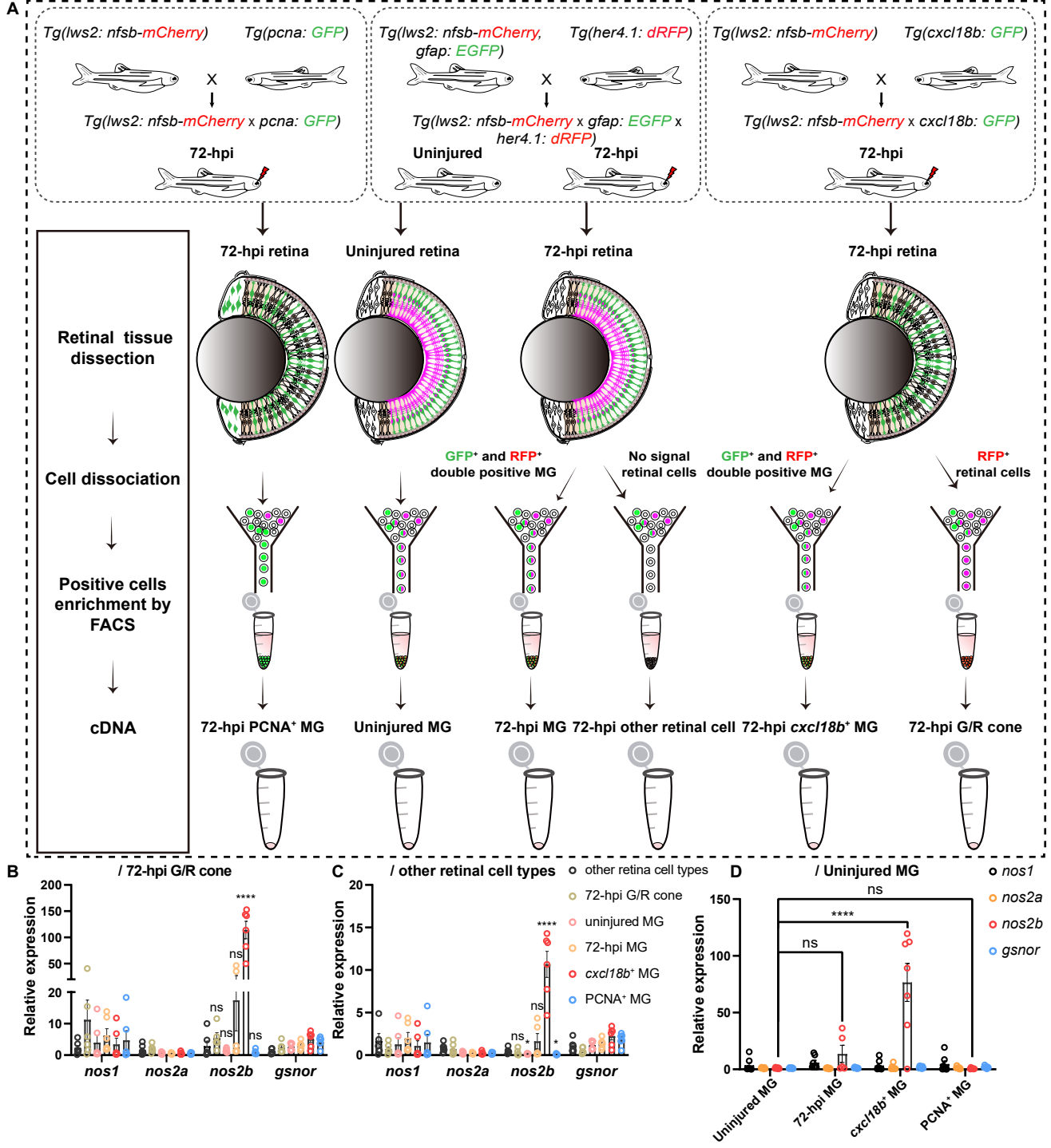
A
Tg(lws2: nfsb-mCherry)
Tg(pcna: GFP)
Tg(lws2: nfsb-mCherry x pcna: GFP)
72-hpi
Tg(lws2: nfsb-mCherry, gfap: EGFP)
Tg(her4.1: dRFP)
Tg(lws2: nfsb-mCherry x gfap: EGFP x her4.1: dRFP)
Uninjured
72-hpi
Tg(lws2: nfsb-mCherry)
Tg(cxcl18b: GFP)
Tg(lws2: nfsb-mCherry x cxcl18b: GFP)
72-hpi
Retinal tissue dissection
Cell dissociation
Positive cells enrichment by FACS
cDNA
72-hpi retina
Uninjured retina
72-hpi retina
72-hpi retina
GFP+ and RFP+ double positive MG
No signal retinal cells
GFP+ and RFP+ double positive MG
RFP+ retinal cells
72-hpi PCNA+ MG
Uninjured MG
72-hpi MG
72-hpi other retinal cell
72-hpi cxcl18b+ MG
72-hpi G/R cone
B
/ 72-hpi G/R cone
Relative expression
nos1
nos2a
nos2b
gsnor
C
/ other retinal cell types
other retina cell types
72-hpi G/R cone
uninjured MG
72-hpi MG
cxcl18b+ MG
PCNA+ MG
D
/ Uninjured MG
nos1
nos2a
nos2b
gsnor
Uninjured MG
72-hpi MG
cxcl18b+ MG
PCNA+ MG

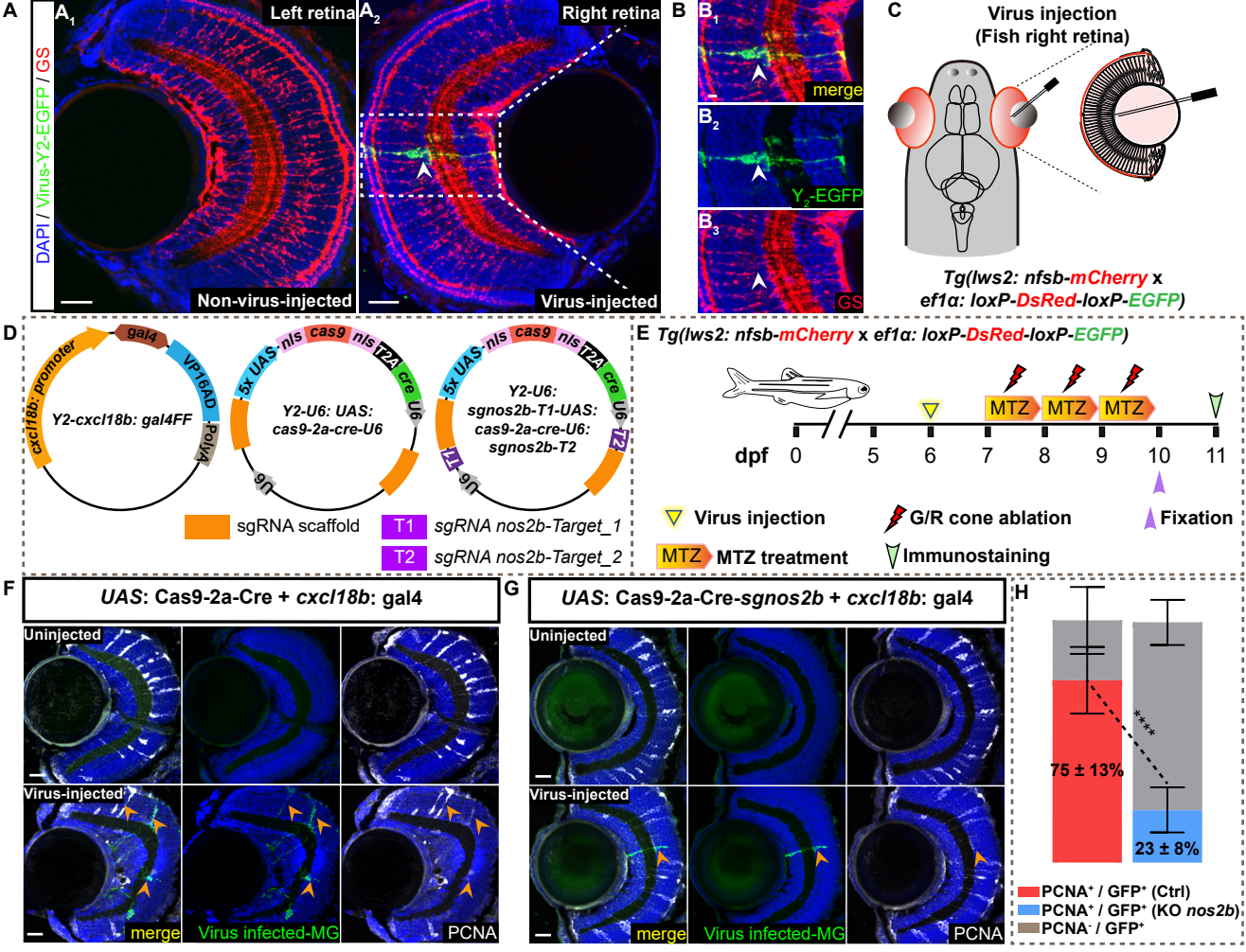
A
A1
Left retina
A2
Right retina
DAPI / Virus-Y2-EGFP / GS
Non-virus-injected
Virus-injected
B
B1
merge
B2
Y2-EGFP
B3
GS
C
Virus injection
(Fish right retina)
Tg(lws2: nfsb-mCherry x
ef1α: loxP-DsRed-loxP-EGFP)
D
gal4
VP16AD
PolyA
cxcl18b: promoter
Y2-cxcl18b: gal4FF
5x UAS
nls
cas9
nls
T2A
cre
U6
Y2-U6: UAS:
cas9-2a-cre-U6
Y2-U6:
sgnos2b-T1-UAS:
cas9-2a-cre-U6:
sgnos2b-T2
T1
T2
sgRNA scaffold
T1 sgRNA nos2b-Target_1
T2 sgRNA nos2b-Target_2
E Tg(lws2: nfsb-mCherry x ef1α: loxP-DsRed-loxP-EGFP)
MTZ
dpf 0 5 6 7 8 9 10 11
Virus injection
G/R cone ablation
Fixation
MTZ treatment
Immunostaining
F
UAS: Cas9-2a-Cre + cxcl18b: gal4
Uninjected
Virus-injected
merge
Virus infected-MG
PCNA
G
UAS: Cas9-2a-Cre-sgnos2b + cxcl18b: gal4
Uninjected
Virus-injected
merge
Virus infected-MG
PCNA
H
75 ± 13%
23 ± 8%
***
PCNA+ / GFP+ (Ctrl)
PCNA+ / GFP+ (KO nos2b)
PCNA- / GFP+

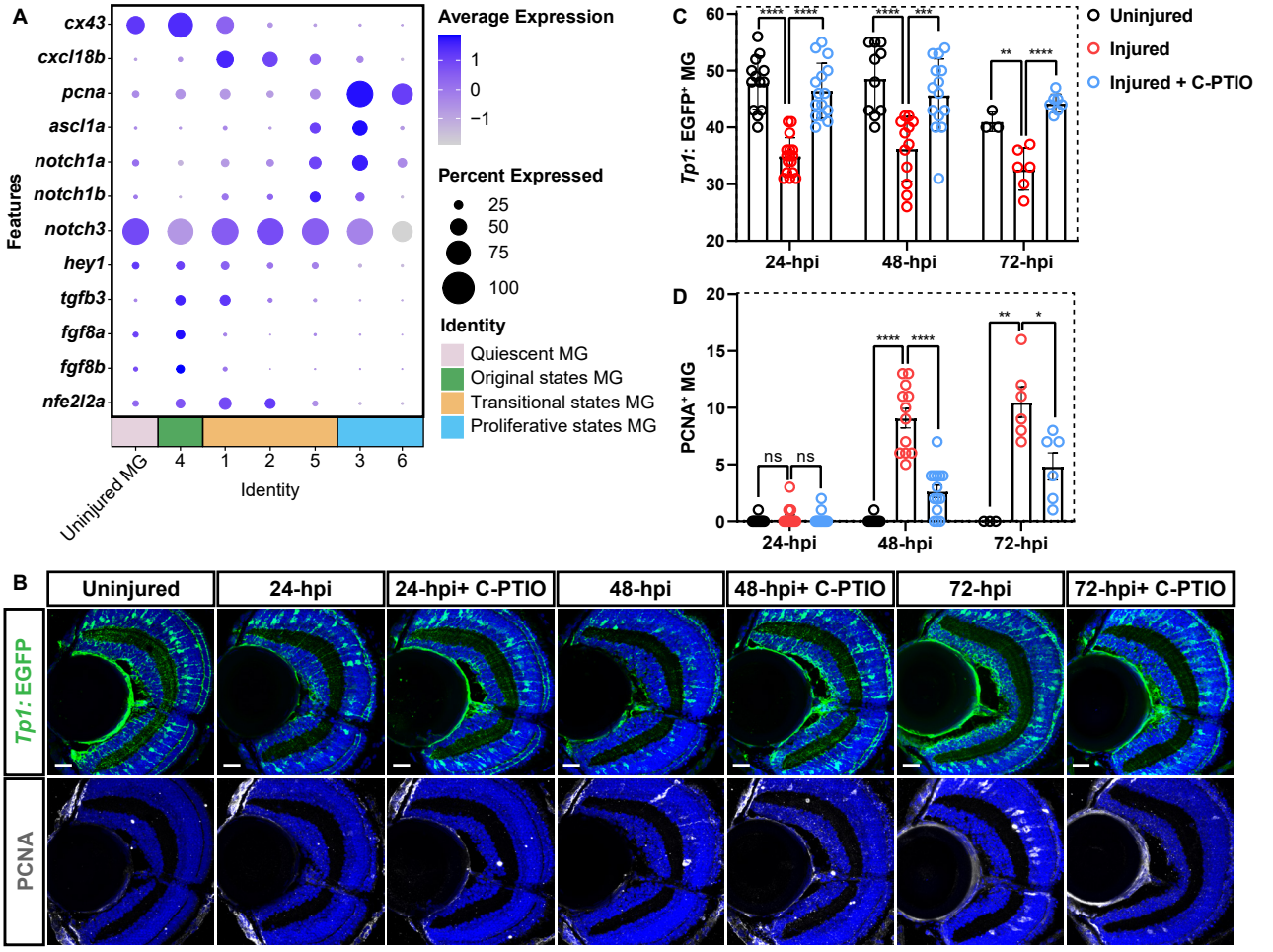
A
Features
cx43
cxcl18b
pcna
ascl1a
notch1a
notch1b
notch3
hey1
tgfb3
fgf8a
fgf8b
nfe2l2a
Uninjured MG
4
1
2
5
3
6
Identity
Average Expression
1
0
−1
Percent Expressed
25
50
75
100
Identity
Quiescent MG
Original states MG
Transitional states MG
Proliferative states MG
C
Tp1: EGFP+ MG
24-hpi
48-hpi
72-hpi
Uninjured
Injured
Injured + C-PTIO
D
PCNA+ MG
ns
B
Uninjured
24-hpi
24-hpi+ C-PTIO
48-hpi
48-hpi+ C-PTIO
72-hpi
72-hpi+ C-PTIO
Tp1: EGFP
PCNA